CUMENTATION PAGE

Form Approved
OMB No 0704-0188

1. AGENCY USE ONLY (Leave blank)	2. REPORT DATE	3. REPORT TYPE AND DATES COVERED
	1992	FINAL 1 SEPT 90 - 28 FEB 94

4. TITLE AND SUBTITLE

HIGH TEMPERATURE FRACTURE MECHANISMS IN METALLIC MATRIX COMPOSITES PRODUCED BY SOLIDIFICATION TECHNIQUES

5. FUNDING NUMBERS

61103D 3484 S2

6. AUTHOR(S)

EARTHMAN, JAMES C.
LAVERNIA, ENRIQUE J.

7. PERFORMING ORGANIZATION NAME(S) AND ADDRESS(ES)

Univ of California, Irvine
Room 115, Administration Bldg.
Irvine, CA 92717-1875

8. PERFORMING ORGANIZATION REPORT NUMBER

9. SPONSORING/MONITORING AGENCY NAME(S) AND ADDRESS(ES)

AFOSR/NC
Building 410, Bolling AFB DC
20332-6448

10. SPONSORING/MONITORING AGENCY REPORT NUMBER

AFOSR 90-0366

AFOSR-TR- 94 0482

11. SUPPLEMENTARY NOTES

12a. DISTRIBUTION/AVAILABILITY STATEMENT

APPROVED FOR PUBLIC RELEASE; DISTRIBUTION IS UNLIMITED.

A

12b. DISTRIBUTION CODE

13. ABSTRACT *(Maximum 200 words)*

Basic studies of solidification processing and high temperature deformation that have a critical effect on fracture in intermetallic materials have been conducted.

A study was undertaken with the objective of assessing the correlation between point counting, image analysis and acid analysis, for the determination of the volume fraction of particulate reinforcement in MMCs. In order to illustrate the effects of reinforcement and matrix composition on the results, two different matrices (Al and Ni_3Al) and two types of reinforcing particulates (SiC and TiB_2) were selected for the present study.

14. SUBJECT TERMS	15. NUMBER OF PAGES
HIGH TEMPERATURE FRACTURE; METAL MATRIX COMPOSITES SOLIDIFICATION PROCESSING	47
	16. PRICE CODE

17. SECURITY CLASSIFICATION OF REPORT	18. SECURITY CLASSIFICATION OF THIS PAGE	19. SECURITY CLASSIFICATION OF ABSTRACT	20. LIMITATION OF ABSTRACT
UNCLASSIFIED	UNCLASSIFIED	UNCLASSIFIED	

Final Technical Report

for

AFOSR Grant No. 90-0366

HIGH TEMPERATURE FRACTURE MECHANISMS IN METALLIC MATRIX COMPOSITES PRODUCED BY SOLIDIFICATION TECHNIQUES

Submitted to:

Dr. Charles H. Ward
Department of the Air Force
Directorate of Electronic and Materials Sciences
Air Force Office of Scientific Research
Bolling Air Force Base, Building 410
Washington D.C. 20332

Submitted by:

James C. Earthman and Enrique J. Lavernia
Materials Section
Department of Mechanical and Aerospace Engineering
University of California
Irvine, California 92717

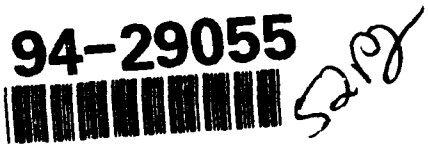

This research was supported by the Air Force Office of Scientific Research (AFOSR) under Grant No. AFOSR-90-0366. Approved for public release; distribution unlimited.

TABLE OF CONTENTS

EXECUTIVE SUMMARY

Basic studies of solidification processing and high temperature deformation that have a critical effect on fracture in intermetallic materials have been conducted. The solidification work has led to a better understanding of the processes that control interfacial reactions in the experimental materials. A detailed examination of the deformation and damage behavior of a spray deposited Ni_3Al matrix composite has resulted in a better understanding of the role of reinforcement particulates under creep conditions. This knowledge was needed to develop improved methods for enhancing the high temperature properties of metallic matrix composites as well as to create better methods for predicting creep fracture in this important class of materials.

The principal developments reported here can be grouped into three categories: composite characterization, solidification processing, and an analysis of deformation and damage mechanisms that control high temperature fracture in a Ni_3Al matrix composite; these are discussed in three sections in the main body of this report.

A study was undertaken with the objective of assessing the correlation between point counting, image analysis and acid analysis, for the determination of the volume fraction of particulate reinforcement in MMCs. In order to illustrate the effects of reinforcement and matrix composition on the results, two different matrices (Al and Ni_3Al) and two types of reinforcing particulates (SiC and TiB_2) were selected for the present study.

In order to investigate the accuracy of each technique, a statistical analysis of variance was used to study the measurement results for $(SiC+TiB_2)_p$-Ni_3Al composites. The results of the analyses suggest that all three methodologies utilized in the present investigation can provide reasonably accurate volume fraction determination. The most significant difference between the three techniques evaluated in the present study involves the time required to perform the volume fraction measurements. The image analysis technique was substantially faster in producing results with nearly the same accuracy. In addition, the time required to obtain the results can be reduced further by programming this system to perform all measurements automatically once the optimum analysis procedure is determined. Fully automated measurements can be conducted in a matter of seconds for each photomicrograph or sampling field, while the point counting method described in ASTM E562-83 requires several minutes for each sampling field. This difference in time multiplied by the recommended minimum number of 30 fields for each volume fraction determination results in a considerable time savings using the image analysis system. In addition, whereas image analysis and point counting can be accurately accomplished using a standardized procedure, acid analysis will depend on the type of matrix involved and is very sensitive to the experimental procedure. For example, during the filtration process, extreme care must be taken in order to avoid accidental loss of filtrate, since this will void the results of the test. Furthermore, it

is important that the filtrate be allowed to dry sufficiently before its final weighing, since the presence of an aqueous component will increase the mass of the filtrate. In the case of the $(SiC+TiB_2)_p$-Ni_3Al composite, for example, a series of trial experiments suggested that it was necessary to allow the samples to dry at room temperature for a period of one week, before final weighing was conducted. In summary, the results of the present study show that all three methodologies can provide reasonably accurate volume fraction determinations; however, image analysis may be preferred over the other two techniques as a result of the time savings realized.

The mechanisms governing the morphological changes in the microstructure of spray atomized and deposited Ni_3Al and a Ni_3Al matrix composites (IMCs) were studied, with particular emphasis on the formation of spheroidal grains and the interfacial interaction between Ni_3Al and ceramic reinforcements. The various microstructural features present that are in the spray deposited material were rationalized on the basis of thermal energy considerations. The formation of spheroidal grains was proposed to evolve from: a) the homogenization of dendrites that did not deform extensively during deposition; and b) the growth and coalescence of deformed or fractured dendrite fragments. The formation of an interfacial reaction zone between Ni_3Al and TiB_2 in the deposited Ni_3Al IMC was proposed to be activated by the thermal energy associated with a sluggish cooling behavior during deposition. Support for this suggestion was provided by experimental results and numerical analyses which show that the microstructures of Ni_3Al and Ni_3Al IMC are exposed to a high temperature anneal during deposition.

High temperature fracture mechanisms were studied in a spray deposited and extruded Ni_3Al composite reinforced with both TiB_2 and SiC particulates. For this investigation, creep rupture specimens were tested under constant stresses ranging from 180 to 350 MPa in vacuum at 1033K. Metallographic examinations of tested specimen cross-sections reveal that the high temperature fracture is primarily manifested by the nucleation and growth of cavities on the grain boundaries of the Ni_3Al matrix as opposed to cavitation on the Ni_3Al/TiB_2 interfaces. The results also suggest that the cavities nucleate at fine carbides lying on the Ni_3Al grain boundaries which result from the decomposition of the SiC_p. This observation accounts for the relatively short rupture times for the $Ni_3Al/SiC/TiB_2$ IMC compared to that for monolithic Ni_3Al. The overall results indicate that a Ni_3Al matrix composite containing only TiB_2 could have a resistance to high temperature fracture that is comparable to monolithic Ni_3Al with the advantages of higher a strength-to-weight ratio and stiffness provided by the reinforcement.

RESEARCH REPORT

I. A Comparison of Techniques for Determining the Volume Fraction of Particulates in Metal Matrix Composites

A. Introduction

The attractive physical and mechanical properties that can be achieved with metal matrix composites (MMCs), such as high modulus, strength, and thermal stability have been documented extensively [1-4]. MMCs combine the metallic properties of the matrix (ductility and toughness) with the ceramic properties of the reinforcement (high strength and high modulus). Interest in MMCs for aerospace, automotive and other structural applications has increased over the last five years, as a result of the availability of relatively inexpensive ceramic reinforcements and the development of various processing routes which result in reproducible microstructures and properties [4]. The reinforcements may be in the form of continuous fibres, whiskers, platelets, or particulates. In spite of the fact that the mechanical properties of discontinuously reinforced (particulates) MMCs are reportedly inferior to those of MMCs reinforced with continuous fibers or short whiskers [5], particulate reinforced MMCs offer several advantages. For example, particulate reinforced MMCs can be readily formed by standard or near standard manufacturing techniques, rendering them economically attractive [4]. Furthermore particulate reinforced MMCs outperform their monolithic counterparts in terms of hardness and modulus, particularly when considering applications which do not involve extreme loading or elevated temperatures.

The physical and mechanical behavior of particulate reinforced MMCs depend, not only on the type of reinforcement, but also on the quantity (normally referred to as volume fraction) and distribution of reinforcing phases present in the metal matrix. For example, the volume fraction dependance of the tensile strength and ductility in particulate reinforced MMCs is well documented [5]. There are various experimental methods available that can be readily utilized to determine the reinforcement volume fraction in MMCs. The most widely utilized techniques are: manual point counting, image analysis and acid analysis. However, a review of the available scientific literature reveals that there is limited information on the accuracy of these three methodologies, particularly when applied to particulate reinforced MMCs with differing matrix characteristics. Therefore, the present study was undertaken with the objective of assessing the correlation between point counting, image analysis and acid analysis, for the determination of the volume fraction of particulate reinforcement in MMCs. In order to illustrate the effects of reinforcement and matrix composition on the results, two different matrices (Al and Ni_3Al) and two types of reinforcing particulates (SiC and TiB_2) were selected for the present study.

B. Experimental

The two different metal-matrix composites investigated in the present study are an aluminum based MMC, and a nickel aluminide (Ni_3Al) based MMC. The first composite is a 6061 aluminum matrix containing approximately 40 vol.% of SiC particulates (SiC_p), and was obtained from the Advanced Composite Materials Corporation (Greer, SC). This material was processed by a powder metallurgy route, consisting of blending fine atomized matrix powders with the reinforcing particulates, followed by canning, pressing and hot extrusion [6, 7]. The microstructure of the SiC_p-Al composite is shown in Fig. 1, and consists of a fairly homogeneous distribution of SiC_p, typically less than 10 μm, in the Al matrix. It is also worth noting from this figure that the SiC_p exhibited an aspect ratio slightly greater than unity.

The second composite is a Ni_3Al intermetallic compound containing both SiC and TiB_2 particulates with a combined volume fraction of approximately 10%. This intermetallic matrix composite (IMC) was prepared by a spray atomization and deposition approach, involving atomization of the matrix material while simultaneously co-injecting the reinforcing particulates, followed by deposition onto a substrate [8, 9]. The microstructure of the $(SiC+TiB_2)_p$-Ni_3Al composite is shown in Fig. 2, where the reinforcing particulates can be seen to be randomly distributed within the matrix. It was not possible to differentiate between the SiC and TiB_2 particulates in the photomicrograph strictly on the basis of size and morphology. However, it is worth noting that the average size of the SiC and TiB_2 particulates is approximately 3 μm and 15 μm, respectively, suggesting that the large particulates seen in Fig. 2 are TiB_2,.

The volume fraction of ceramic reinforcement in the Al-matrix and the Ni_3Al-matrix materials was determined using three different techniques: (1) point counting, (2) image analysis, and (3) acid dissolution. The specimens for point counting and image analysis were prepared using standard metallographic techniques. The SiC_p-Al composite was etched with Keller's reagent, whereas the $(SiC+TiB_2)_p$-Ni_3Al composite was etched with Marble's regent (10g CuSO4: 50ml HCl: 50ml H_2O). Over etching was undertaken to enhance the contrast difference between the matrix and the ceramic reinforcement. Following etching, three photomicrographs were taken by scanning electron microscopy for each composite to conduct the point counting and image analysis.

Point counting was performed in accordance with ASTM standard E562-83 [10]. Accordingly, a transparency containing a square grid pattern with a 25 point grid size was placed over a photomicrograph of the composite material. The same grid size was used for both the Al-matrix and the Ni_3Al-matrix composites. The volume fraction of ceramic reinforcement was determined using the procedure specified in sections 7 and 8 of ASTM standard E562-83 [10]. This methodology involves counting the number of grid intersections with the ceramic particles and

dividing them by the total number of points in the grid. In order to minimize measurement errors, thirty sampling fields were measured on each photomicrograph. The average volume fraction of SiC_p in the Al-matrix and $(SiC+TiB_2)_p$ in the Ni_3Al-matrix was determined using the aforementioned procedure, and is listed in Table 1 together with the corresponding deviation of estimation.

Image analysis was accomplished using an ImageSet image analysis system developed by Dapple Systems Incorporated. This procedure involved computerized analysis of a digitized image obtained from the same photomicrographs of the etched SiC_p-Al and $(SiC+TiB_2)_p$-Ni_3Al composites. The average volume fraction of SiC_p in the Al-matrix and $(SiC+TiB_2)_p$ in the Ni_3Al-matrix determined using image analysis are listed in Table 1.

The third method used to determine the volume fraction of ceramic reinforcement in the two composite materials involved acid dissolution of the matrix phase. For the SiC_p-Al composite a concentrated HCl solution (80 vol.% HCl-20 vol.% H_2O) was used to dissolve the Al-matrix. It was experimentally noted that Al is soluble in such a solution, whereas SiC is insoluble. Accordingly, the following procedure was adopted for the present investigation. A SiC_p-Al composite sample was cleaned using acetone, weighed (m_c = mass of the composite) and placed in the concentrated HCl solution for 72 hours, and stirred periodically. Subsequently, the solution containing the dissolved Al and insoluble SiC was filtered with distilled water. The insoluble material obtained from this step was then air dried at room temperature and weighed (m_{SiC}); the insoluble material was assumed to be only SiC. The volume fraction of SiC, v_{SiC}, was calculated using the following relationship [11]:

$$v_{SiC} = \frac{m_{SiC}/\rho_{SiC}}{\frac{m_c - m_{SiC}}{\rho_{Al}} + \frac{m_{SiC}}{\rho_{SiC}}} \qquad (1)$$

where ρ_{Al} is the density of Al equal to 2.70 gm/cm^3 and ρ_{SiC} is the density of SiC equal to 3.22 gm/cm^3 [4, 7]. In order to minimize experimental error, the acid dissolution method was repeated with five different SiC_p-Al composite samples. The average volume fraction of SiC_p in the Al-matrix was determined using the aforementioned procedure, and is listed in Table 1 together with the corresponding standard deviation.

A procedure, similar to the one described for the SiC_p-Al composite, was employed for the $(SiC+TiB_2)_p$-Ni_3Al composite, with the exception that a 30 vol.%HCl-50 vol.% HNO_3-20 vol.% H_2O solution was used to dissolve the Ni_3Al-matrix. It was experimentally observed that the Ni_3Al matrix is soluble in a such solution whereas, the TiB_2 and SiC particulates are insoluble. In addition, prior to acid dissolution, the volume of the $(SiC+TiB_2)_p$-Ni_3Al composite, V_{comp}, was

determined on the basis of Archimedes' principle, with distilled water as the liquid. Following acid dissolution and drying, the weight of the insoluble product was recorded; the insoluble material was assumed to be only TiB_2+SiC. The volume fraction of ceramic reinforcement, v_{TiB_2+SiC}, was then calculated from the following equations:

$$V_{Ni_3Al} = \frac{m_c - m_{TiB_2+SiC}}{\rho_{Ni_3Al}} \qquad (2)$$

where V_{Ni_3Al} is the volume of Ni_3Al, m_c is the mass of the $(SiC+TiB_2)_p$-Ni_3Al composite, m_{TiB_2+SiC} is the mass of the ceramic reinforcement (insoluble product) and ρ_{Ni_3Al} is the density of Ni_3Al equal to 7.50 gm/cm^3 [12] and

$$v_{TiB_2+SiC} = \left[1 - \frac{V_{Ni_3Al}}{V_{comp}}\right] \qquad (3)$$

The acid dissolution procedure was repeated for three different $(SiC+TiB_2)_p$-Ni_3Al composite samples. The average volume fraction of TiB_2+SiC in the Ni_3Al-matrix was determined using Equations 2 and 3 and is listed in Table 1, together with the corresponding standard deviation.

C. Results and Discussion

In order to investigate the accuracy of each technique, a statistical analysis of variance (ANOVA) [13] was used to study the measurement results for the $(SiC+TiB_2)_p$-Ni_3Al composite. The results of the analysis are summarized in Table 2, where F^* is the calculated factor effect risk and $F_{0.95}$ is the 95% confidence F-value. If $F^* > F_{0.95}$, then there is 95% confidence that the measurement techniques used will influence the volume fraction results. Inspection of the results shown in Table 2, however, shows that, $F^* < F_{0.95}$, suggesting that all three methodologies utilized in the present investigation can provide reasonably accurate volume fraction determination. The most significant difference between the three techniques evaluated in the present study involves the time required to perform the volume fraction measurements. The image analysis technique was substantially faster in producing results with nearly the same accuracy. In addition, the time required to obtain the results can be reduced further by programming this system to perform all measurements automatically once the optimum analysis procedure is determined. Fully automated measurements can be conducted in a matter of seconds for each photomicrograph or sampling field, while the point counting method described in ASTM E562-83 [10] requires several

minutes for each sampling field. This difference in time multiplied by the recommended minimum number of 30 fields for each volume fraction determination results in a considerable time savings using the image analysis system. In addition, whereas image analysis and point counting can be accurately accomplished using a standardized procedure, acid analysis will depend on the type of matrix involved and is very sensitive to the experimental procedure. For example, during the filtration process, extreme care must be taken in order to avoid accidental loss of filtrate, since this will void the results of the test. Furthermore, it is important that the filtrate be allowed to dry sufficiently before its final weighing, since the presence of an aqueous component will increase the mass of the filtrate. In the case of the $(SiC+TiB_2)_p$-Ni_3Al composite, for example, a series of trial experiments suggested that it was necessary to allow the samples to dry at room temperature for a period of one week, before final weighing was conducted.

D. Summary

In summary, the results of the present study show that all three methodologies can provide reasonably accurate volume fraction determinations; however, image analysis may be preferred over the other two techniques as a result of the time savings realized.

E. References

1. Y. Flom and R.J. Arsenault, Interfacial bond strength in an aluminium alloy 6061-SiC composite, *J. Mater. Sci. Eng.* 77: 191-197 (1986).
2. V.C. Nardone and K.W. Prewo, On the strength of discontinuous silicon carbide reinforced aluminum composites, *Scr. Metall.* 20: 43-48 (1986).
3. T.G. Nieh, Creep rupture of a silicon carbide reinforced aluminum composite, *Metall. Trans. A* 15: 139-146 (1984).
4. I.A. Ibrahim, F.A. Mohamed and E.J. Lavernia, Particulate reinforced metal matrix composites: a review, *J. Mater. Sci.*, 26: 1137-1156 (1991).
5. D.L. McDanels, Analysis of stress-strain, fracture, and ductility behavior of aluminum matrix composites containing discontinuous silicon carbide reinforcement, *Metall. Trans. A*, 16: 1105-1115 (1985).
6. Jack Pickens, Advanced Composites Materials Corporation, Greer, South Carolina, private communication, 1989.
7. A.L. Geiger and M. Jackson, Low expansion MMCs boost avionics, *Adv. Mater. Process*, 7: 23-30 (1989).

8. M. Gupta, F.A. Mohamed and E.J. Lavernia, Solidification behavior of Al-Li-SiC processed using variable co-deposition of multi-phased materials, *Mater. & Manuf. Processes*, 5 (2): 165-196 (1990).
9. M. Gupta, F.A. Mohamed and E.J. Lavernia, Processing of Al-Li-SiC using variable co-deposition of multi-phased materials, in *Proc. Intl. Symp. on Advances in Processing and Characterization of Ceramic Metal Matrix Composites*, CIM/ICM, 17, H. Mostaghaci ed., Pergamon Press, Aug., (1989) pp. 236-252.
10. Standard Practice for Determining Volume Fraction by Systematic Manual Point Count (E 562-83) in *1984 Annual Book of ASTM Standards*, American Society of Testing Materials, Philadelphia, PA (1984), Vol. 3.03 (Metallography; Nondestructive Testing), pp. 518-524.
11. K.K. Chawla, *Composite Materials*, Springer Verlag, New York (1987), pp. 177-178.
12. J.M. Yang, W.H. Kao, and C.T. Liu, Development of nickel aluminide matrix composites, *J. Mater. Sci. Eng.*, A107: 81-91 (1989).
13. N.P. Cheremisinoff and P.N. Cheremisinoff, Engineering Mathematics and Statistics, Technomic Publishing Company, Inc., Lancaster, PN (1989), pp. 81-90.

Table 1. Volume Fraction of Ceramic Reinforcement

Metal Matrix Composite	Measurement Technique		
	Point Counting	*Image Analysis*	*Acid Dissolution*
SiC_p in 6061 Al	0.43 ± 0.035*	0.45 ± 0.04**	0.49 ± 0.03**
$(SiC+TiB_2)_p$ in Ni_3Al	0.13 ± 0.012*	0.11 ± 0.04**	0.14 ± 0.02**

* Deviation of estimate σ, given by $\sigma = S/\sqrt{n}$, where S is the standard deviation of the total measurements and n is the number of samples, i.e., 3.

** Standard deviation of samples.

Table 2. Analysis of variance (ANOVA) results for the volume fraction measurement values from three different methods for the $(SiC+TiB_2)_p$-Ni_3Al composite.

source of variations	degrees of freedom	sum of squares SS	mean squares MS	factor effect risk F*
technique	2	1.6×10^{-3}	8.0×10^{-4}	1.02†
error	9	4.7×10^{-3}	7.8×10^{-4}	

† Compare this value with $F_{0.95}(2, 9) = 5.14$.

Fig. 1. Scanning electron micrograph showing the distribution of SiC particulates in the 6061 Al matrix.

Fig. 2. Scanning electron micrograph showing the distribution of SiC and TiB_2 particulates in the Ni_3Al matrix.

II. Microstructure Evolution in Ni_3Al and Ni_3Al Matrix Composites During Spray Atomization and Deposition

A. Introduction

Intermetallic compounds are attractive candidate materials in applications that require elevated temperature stability. Of the various types of intermetallic compounds available, the $L1_2$ structure, long-range ordered Ni_3Al system has received considerable attention. The yield strength of this material increases with increasing temperature, up to 600 °C [1, 2]. Moreover, microalloying with B dramatically improves the grain boundary cohesion of polycrystalline Ni_3Al, thereby providing significant improvements in ductility [1-4]. The density of Ni_3Al is lower than those of traditional Ni-base superalloys because of the high content of Al. In addition, unlike Ti-based intermetallics which require sophisticated processing techniques due to their high reactivity, Ni_3Al may be manufactured by conventional processing. More recently, investigators have sought to achieve further improvements in the properties of intermetallics, by utilizing them in intermetallic matrix composites (IMCs) containing continuous or discontinuous ceramic reinforcements [5-8].

Over the past decade, spray atomization and deposition has attracted considerable attention as a viable processing alternative for structural materials, and has been successfully applied to numerous alloy systems [9-12]. This synthesis methodology essentially refers to a two-step process: the energetic disintegration of a molten material by inert gas jets into micron-sized droplets (atomization) and the subsequent deposition of the mixture of solid, liquid, and partially solidified droplets on a substrate surface (deposition) [13]. The droplets eventually collect as a coherent preform, the microstructure of which is largely dictated by the solidification conditions of the droplets during impact. This synthesis methodology offers a potentially attractive manufacturing route for several reasons. First, the highly efficient heat extraction during atomization ensures the maintenance of relatively low processing temperatures which limits large scale segregation and coarsening phenomena. Second, the inert conditions required for atomization and deposition minimize surface oxidation and other deleterious surface reactions. In addition, spray atomization and deposition may potentially be used for near net shape manufacturing of difficult-to-form materials, such as intermetallic compounds and discontinuously reinforced metal matrix composites [14-16].

Detailed study of the solidification mechanisms that govern the evolution of microstructure during spray atomization and deposition is made highly complex by the extreme differences in thermal environment before and after impact of the droplets onto the deposition surface. During atomization, the violent extraction of thermal energy by the atomization gas promotes the formation of highly refined microstructures [17]. In contrast, the solidification conditions after the

distribution of droplets arrives on the deposition surface are governed by relatively sluggish cooling rates [18, 19]. The microstructure of spray atomized and deposited materials is generally reported to exhibit spheroidal or "equiaxed" grains, a feature that is consistently observed regardless of alloy composition. Recently, a comprehensive study of this phenomena has been reported [20]. Moreover, recent work on the interfacial behavior in metal matrix composites processed spray atomization, co-injection and deposition has revealed some interesting insights into the thermal and solidification conditions that govern microstructural evolution [21, 22].

In view of the aforementioned findings, the objective of the present work was to summarize recent findings on the mechanisms that govern the morphological changes in the microstructure of spray atomized and deposited Ni_3Al and Ni_3Al IMCs, with particular emphasis on the formation of spheroidal grains and interfacial interactions between Ni_3Al and ceramic reinforcements. Accordingly, the evolution of microstructure in monolithic Ni_3Al and Ni_3Al IMCs is discussed in light of results obtained from numerical simulations, experimental results and detailed microstructural studies.

B. Experimental Procedures

The alloys used in these studies were provided by the Oak Ridge National Laboratory (Oak Ridge, TN, U.S.A.) under the designation IC-50 and IC-396. The nominal compositions of the as-cast IC-50 and IC-396 Ni_3Al were (in atomic percent) 21.8 Al, 0.3 Zr, 0.09 B, bal. Ni, and 16.3 Al, 8.1 Cr, 0.5 Zr, 1.7 Mo, 0.03 B, bal. Ni, respectively. Microalloying with B and Zr has been shown to improve the grain boundary cohesion of polycrystalline Ni_3Al [1-5], whereas Cr and Mo reportedly improve the high temperature resistance of these alloys. TiB_2 (C32 type, hexagonal structure) equiaxed particulates were selected as the reinforcements in the Ni_3Al IMC and exhibited a typical size of 10 μm [21, 22].

The synthesis of Ni_3Al/TiB_2 IMC by spray atomization and deposition involves the following procedure. The matrix material (Ni_3Al) is superheated to a preselected temperature of 1823 K and delivered to an atomizer, where it is disintegrated into a Gaussian distribution of micron-sized droplets using nitrogen gas at a dynamic pressure of 2.41 MPa. The mass flow rates of the atomizing gas and melt are 0.078 and 0.022 kg/s, respectively [21, 22]. Simultaneously, two jets of TiB_2 particulates positioned at 180° from each other are injected into the atomized spray at a previously selected flight distance, i.e., 15.2 cm. Following co-injection, the mixture of rapid quenched, partially solidified Ni_3Al droplets with interdispersed ceramic particulates is deposited onto a water-cooled copper substrate (placed at a flight distance of 25.4 cm), eventually collecting as a coherent preform. Both particulate injection and substrate distances are typically determined on the basis of the numerical analysis of the temperature and fraction of solid contained in the

atomized matrix droplets; a more thorough discussion of the experimental process and the numerical results is available elsewhere [13, 20]. To avoid extensive oxidation of the Ni_3Al matrix during processing, the experiment is conducted inside an environmental chamber. The chamber is evacuated down to a pressure of 200 Pa (~1.5 torr) and backfilled with inert gas of nitrogen prior to melting and atomization. To process the monolithic Ni_3Al, no reinforcing particulates are injected into the atomization spray and all other processing parameters are identical to those used for the Ni_3Al/TiB_2 IMC experiment.

The geometry of spray deposited Ni_3Al and Ni3Al IMC often exhibits a contour akin to the Gaussian distribution of droplets impacting on the substrate [23], shown in Fig. 1, although this geometry may be readily modified by displacing the substrate during deposition. Fig. 1 also shows the positions of three thermocouples that are placed at various distances from the water cooled substrate to systematically monitor the temperature of the material during deposition. Thermocouple I, type K (Chromel vs. Alumel, temperature range 273 ~ 1523 K), is positioned the substrate surface. Thermocouples II and III, type C (Tungsten-5%Rhenium vs. Tungsten-26%Rhenium, temperature range 273 ~ 2593 K), are placed at 5 mm and 10 mm above the substrate surface, respectively. To minimize any effects derived from the lag time of the thermocouples, no ceramic protection tubes were used in these experiments [20]. Moreover, it is worth noting that the lag time of these particular thermocouples is approximately 0.9 seconds. The temperatures of three thermocouples are simultaneously recorded in a Tracor Westronic 4030 Recorder during the experiment.

To systematically investigate the microstructure of Ni_3Al, sectioned samples from as-deposited Ni_3Al, and atomized Ni_3Al/TiB_2 powders were isothermally annealed under argon inert gas protection at three different temperatures: 1108 K, 1258 K, and 1403 K for given times. The annealed samples were then prepared for microstructural analysis using standard metallographic techniques. Marble's reagent (10g $CuSO_4$: 50ml HCl : 50ml H_2O) was used to etch polished cross-sections of the samples. The changes in microstructure during annealing were carefully studied by Liang et al. [23] examined an ImageSet image analysis system developed by Dapple Systems Incorporated. This procedure permitted the efficient analysis of a large number of samples.

C. Microstructure of As-Deposited Materials

Systematic microstructural characterization studies have been conducted on the spray atomized and deposited IC50-Ni_3Al, paying particular attention to the precise geometric location of the microstructural features of interest [20]. On the basis of these studies, the monolithic Ni_3Al deposit reportedly consists of three regions of differing microstructure, as shown in Fig. 1.

In a region A located near the substrate, the microstructure consisted of densely packed powders that deformed upon impact and thick prior-droplet-boundaries between them, as shown in Fig. 2(a), giving the region a highly irregular appearance. Locally, the microstructure inside the deformed powders consisted of a mixture of deformed and fractured dendrite arms, and what appeared to be dendrite arms aligned perpendicularly to the deposition surface. In general, the microstructural observations made in this region suggest that the droplets were partially solidified during impact onto the deposition surface. It is worth noting that most of the dendrites that were examined in this region appeared to have experienced, either extensive plasticity, and/or fracture. On the basis of work reported elsewhere suggesting that deformed or fractured dendrite arms have a large orientation misfit with the original primary or secondary arms [24], it is reasonable to consider these deformed or fractured dendrite arms as independent grains.

A large fraction of the microstructure in the deposited material, region B, consisted of fine, homogeneous and fully spheroidal grains with an average size of 10.7 μm; this microstructure appeared to be reasonably dense (see Fig. 2(b)), with a porosity of 1.3 vol.% as measured by an Imagine Analysis technique [25].

The microstructure in the exterior region C of the deposited material consisted of a mixture of the microstructural features associated with the other two regions described previously. The spheroidal grains present in this region were not fully developed, and their size distribution was highly heterogeneous. Prior-droplet-boundaries were readily seen in this region although they were thinner than those present in the region near the substrate.

The thermal profile of three locations inside the spray deposited material (see Fig. 1) as measured by Liang et al. [20] shown in Fig. 2 together with the liquidus and solidus temperatures of the Ni_3Al used in the study. The results showed that the temperature at all three locations of the spray deposited material remained below the solidus temperature. From this data it was inferred that the average cooling rate that was associated with the high temperature region ($T > 0.5\ T_m$) was approximately 2.6 K/s.

The microstructure of the spray atomized and deposited IC396-Ni_3Al/TB_2 IMC consisted of relatively homogeneous distribution of reinforced ceramic particulates in the Ni_3Al matrix, as shown in Fig. 4(a). The chemical reactions that occurred at the IC396-Ni_3Al/TiB_2 interface are evident from Fig. 4(b), where the TiB_2 particulates are surrounded by a well defined interfacial reaction zone. This interfacial reaction zone appears to have increased in thickness by consuming both the matrix and the TiB_2 particulates, leading to the formation of two distinct interfacial reaction layers (interfacial reaction layer I and II, as marked "1" and "2" in the figures) [21]. Interfacial reaction layer I formed inside the TiB_2 particulate (i.e., at the TiB_2/reaction zone interface), while interfacial reaction layer II formed in intimate contact with TiB_2 particulate (i.e., at the reaction zone/Ni_3Al matrix interface). Both interfacial reaction layers were highly irregular in

shape. Based on the phase identification analyses, conducted by TEM and EDAX techniques and reported in detail elsewhere [21, 22], the interfacial reaction layer I consisted of a η-Ni_3Ti phase containing Ti, Ni, and Cr with a hexagonal structure ($D0_{24}$-type); and the diffusion of Ni was proposed to be the rate control step in this interfacial reaction. Interfacial reaction layer II showed a very high content of Ni with a low content of Al (Ni-rich phase), however, the electron diffraction pattern analysis indicated that this phase exhibited a $D0_{21}$ crystal structure (Al_3Ni-type) and its formation may be related to the decomposition of the TiB_2 [21]. In addition, the average thickness for the interfacial reaction layer I, was measured as 0.92 μm.

D. Analysis of Microstructure Evolution

Annealing of Spray Atomized and Deposited Materials

Annealing studies, conducted on samples sectioned from region A of spray deposited monolithic Ni_3Al, provided insight into the mechanism governing the transformation of deformed and fractured dendrites into spheroidal grains [20]. The results of these studies showed that the formation of spheroidal grains from dendrite fragments that was observed in samples from region A was qualitatively similar to that reported elsewhere for rapidly solidified Ni_3Al powders [26], although the transformation in the spray deposited material was strongly influenced by the temperature. The microstructure of the spray deposited materials remained almost unchanged during thermal exposure at 1108 K for time up to 10 hours. Although solid-state coarsening of the dendrite fragments was noted to occur in the samples, the microstructure contained interdispersed prior-droplet-boundaries that remained relatively unchanged during annealing.

The microstructure of the spray deposited materials changed dramatically during annealing at 1258 K and 1403 K. Consistent with the results of other investigations on Ni_3Al atomized powders [26], the fine, micron-sized dendritic morphology transformed into a spheroidal grain morphology during annealing, see Fig. 5. Upon annealing at these higher temperatures, the spheroidal grains evolved rapidly at the expense of dendrite fragments. Two distinct mechanisms contributed to the formation of spheroidal grains during annealing [20]: a) the homogenization of dendrites that did not deform extensively during deposition; and b) the growth and coalescence of deformed or fractured dendrite arms. These mechanisms are illustrated schematically in Fig. 6. The observed changes in morphology during annealing resembled the growth of deformation-free grains during recrystallization [27]. In addition, the prior-droplet-boundaries became thinner and lighter. At some locations, these boundaries were supplanted by growing spheroidal grains, such as the one designated 'm' in Fig. 5. A comparison of the microstructural characteristics of these high temperature annealed splat materials with those of region B and C in the as-spray deposited billet suggests that these high-temperature annealed microstructures are similar to the

microstructures shown in region B and C, differing only in grain size and the thickness of prior droplet boundaries. On the basis of the aforementioned results, and to provide insight into the mechanisms governing the formation of spheroidal grains from the growth and coalescence of dendrite fragments, the coarsening behavior of material from region A was carefully monitored during isochronal thermal anneals at three temperatures (1108 K, 1258 K, and 1403 K). Accordingly, changes in the average diameter of both deformed and fractured dendrite arms (as previously discussed, these were treated as independent grains) were measured as a function of annealing time and temperature. The results, shown in Fig. 7, reveal that the growth of the dendrite fragments/spheroidal grains obeys a relationship of the following type: $\{D^2-D_o^2\} \alpha t$, where D is the average diameter of the dendrite fragments or spheroidal grains, and D_o represents the initial average diameter of the dendrite fragments or spheroidal grains. The results also show that the scale of the microstructure rapidly increases with time when the annealing temperature increases.

Similarly, annealing thermal treatments were conducted for Ni_3Al/TiB_2 IMC to investigate the microstructural evolution during spray atomization and deposition [22]. In order to simplify the analysis of the interfacial reaction chemistry, the IC50-Ni_3Al/TiB_2 powder material prepared by spray atomization was selected for the annealing studies. Examination of Ni_3Al/TiB_2 powder samples revealed that the TiB_2 particulates were located at the origin of radially growing cells or dendrites (see Fig. 8(a)). This observation suggested that the TiB_2 particulates may have catalyzed nucleation of the solid phase with concomitant fast solidification velocity in the Ni_3Al droplets [28]. Also evident from the microstructure shown in Fig. 8(a) is the intimate and complete interfacial contact between Ni_3Al matrix and TiB_2 particulates, presumably due to a low wetting contact angle (40° at temperature 1480 °C) between the TiB_2 particulates and the Ni matrix [29], and the absence of an interfacial reaction zone.

Following annealing at elevated temperatures, a distinct interfacial reaction zone formed between the Ni_3Al matrix and the TiB_2 particulates, as shown in Fig. 8(b). On the basis of X-ray, SEM and EDAX studies reported in detail elsewhere [21, 22], this interfacial reaction zone consisted of a η-Ni_3Ti phase, identical to that in the interfacial reaction layer I formed in the spray deposited IC396-Ni_3Al/TiB_2 IMC. Fig. 8(c) shows a schematic diagram, corresponding to the reaction zone from Fig. 8(b), illustrating the determination of the radius of the particulate, R_p, and the radius of the particulate and reaction zone, R_t. The changes in thickness of the interfacial reaction zone formed between Ni_3Al and TiB_2 in atomized Ni_3Al/TiB_2 powders were measured as a function of annealing time and temperature [22]. The results, shown in Fig. 9, reveal that the growth of this interfacial reaction zone obeys a relationship of the following type: $x \alpha t^{1/2}$, where x is the thickness of the interfacial reaction zone and t is the annealing time [22].

Grain Growth Kinetics in Deposited Ni_3Al

In the absence of a cold deformation substructure, grain growth will occur by a grain boundary migration mechanism under the driving force provided by the grain boundary energy of the curved grains [27]. Under these conditions, it has been experimentally determined that the increase in grain diameter will follow a relationship of the type [27] $D^2 - D_o^2 = B \cdot t$, where D is the grain diameter at time t, D_o is the original grain size and B is a constant which value depends on annealing temperature and microstructure of the material. Unlike the phenomenon of grain growth following recrystallization, where deformation free grains nucleate on heavily deformed grains, the coarsening and growth of the spheroidal microstructure observed during spray atomization and deposition occurs exclusively by a grain boundary migration mechanism [20]. Since the migration of the grain boundaries will occur by a thermally activated diffusion mechanism, it then follows that the coefficient B will obey a relationship of the type $B = A \exp(-Q_g/RT)$, where T is the annealing temperature (K); A is a constant related to the type of material; R is the gas constant (8.31 J/mol·K); and Q_g is the activation energy for grain growth. On the basis of the experimental grain growth results obtained during annealing of deposited monolithic Ni_3Al, see Fig. 7, the grain growth kinetics of Ni_3Al spray deposited materials during annealing was suggested as [20]

$$D^2 - D_o^2 = 1.44 \times 10^{11} \cdot e^{-\frac{33800}{T}} \cdot t \qquad [1]$$

With this relationship, the grain size at a certain annealing temperature and time can be predicted; if the annealing temperature and grain size are fixed, the annealing time can also be calculated. For grain sizes of 10, 20 and 30 μm (on the order of the grain sizes present in this study) and a measured initial average dendrite fragment size, D_o, of 6.4 μm, the relationship between the required time and the annealing temperature can be plotted as shown in Fig. 10. An increase in the annealing temperature corresponds to a dramatic decrease in the time needed for the grains in deposited splat materials to grow to a particular size.

An important characteristic of the temperature profile, shown in Fig. 3, is the low cooling rate that is associated with the high temperature period (i.e., $T > 0.5\ T_m$). As stated previously, during high temperature annealing, the rapidly solidified dendrite fragments will coarsen and coalesce to become spheroidal grains. From Fig. 10, the relationship between temperature and annealing time for a constant grain size can be considered to be a log-linear relation, i.e., $\Delta T/\Delta \log \Gamma = M$, where T is the annealing temperature; Γ is the time required to obtain a particular spheroidal grain size at this annealing temperature; M is a constant related to alloy composition and microstructure, and M = -116 K for Ni_3Al [20].

Defining $\dot{T}$ as the cooling rate of the deposited material, then if the temperature of the deposited material decreases from any temperature T_i to $T_i - \Delta T$ under this given cooling rate, the

elapsed time, $\Delta\tau_i$, during a temperature step, ΔT, can be estimated as $\Delta\tau_i = \Delta T/\dot{T}$. At a lower temperature, $T_{i+1} = T_i - \Delta T$, the relative elapsed time, $\Delta\tau_{i+1}$, which accounts for the same grain size as at temperature T_i, will be $(\Delta T/\dot{T})(\Gamma_i/\Gamma_{i+1})$, where Γ_i and Γ_{i+1} are the annealing times required to obtain a constant spheroidal grain size at the corresponding annealing temperatures, T_i and T_{i+1}, respectively. In addition, a time ratio p can be defined here as $p = \Gamma_i/\Gamma_{i+1} = 10^{\Delta T/M}$, then the relative annealing time, $\Delta\tau_{i+1} = \Delta\tau_i\, p$.

Actually the dendrite fragments begin to grow at a temperature, T_0, below the solidus temperature and finish growing at a particular temperature, defined as T_f (at which the grain growth rate is so low that it may be neglected). We may also define a step number, N, of the cooling process as $N = (T_0-T_f)/\Delta T$ [20]. It then follows that an accumulated time, Γ_o, for the deposited material, which is cooled under the given cooling rate $\dot{T}$ to anneal at initial temperature T_0 is

$$\Gamma_o = \sum_{0}^{N-1}\Delta\tau_i = \frac{\Delta T}{\dot{T}}\cdot\sum_{0}^{N-1} p^i \qquad [2]$$

For the conditions described herein, if one selects $T_0 = 1650$ K, $T_f = 1100$ K and $\Delta T = 10$ K, and using the measured cooling rate $\dot{T} = 2.6$ K/s, the value of Γ_o may be determined for different cooling rates. Once Γ_o is obtained, and using grain growth kinetic Eq. 2, grain sizes corresponding to different cooling rates can be calculated as well. The results of these calculations are shown in Fig. 11, for various cooling rates. The good agreement that is evident between the calculated results and the experimentally determined data point provide further support to the suggestion that the formation of spheroidal grains during deposition occurs via the growth and coalescence of dendrite fragments during annealing. It is worth noting that the relationship between spheroidal grain size and cooling rate in the deposited material, shown in Fig. 11, follows a power equation of the type $d_{sph} = 15.2\ \dot{T}^{-0.35}$.

Interfacial Behavior in Deposited Ni_3Al/TiB_2 IMC

During the annealing of atomized Ni_3Al/TiB_2 powders, the thickness of the interfacial reaction zone between Ni_3Al and TiB_2 increased with annealing temperature and time, as shown in Fig. 9. It has been well established that the interfacial behavior in these types of materials can be readily described by a phenomenological equation of the type [30], $x(t, T) = x_0 + kt^n$, where x(t, T) represents the thickness of the interfacial reaction zone as a function of annealing time t and annealing temperature T; x_0 represents the initial thickness of the reaction zone (the value is zero in the atomized powder); and k is a reaction rate coefficient related to the annealing temperature. As shown in Figure 3, the magnitude of the reaction exponent, n, can be readily determined as 0.5. This parabolic relationship between thickness of reaction zone and annealing time suggests that

diffusion through the reaction zone was the rate-limiting step for the growth of the interfacial reaction products [30].

Based on the analysis of the measured thickness of the interfacial reaction zone between Ni_3Al/TiB_2, and the mechanism of interfacial reaction controlled by the diffusion activation process, the time and temperature dependence of the thickness of the interfacial reaction zone formed between Ni_3Al/TiB_2 was proposed as [22]

$$x(t,T) = 12.8 \cdot \exp(-7400/T) \cdot t^{1/2} \qquad [3]$$

Eq. 3 describes the interfacial reaction kinetics between Ni_3Al and TiB_2 and is similar to Eq. 1 describing grain growth in deposited monolithic Ni_3Al. If we assume that the cooling rate experienced by Ni_3Al/TiB_2 IMC is similar to that measured for monolithic Ni_3Al, then a relationship between the thickness of the interfacial η-Ni_3Ti phase and the cooling rate during deposition may be readily using a procedure similar to the one described herein for monolithic Ni_3Al (see Eq. 1-2). The results of these calculations are shown in Fig. 11, where they are compared to the experimental findings obtained for as-deposited IC396-Ni_3Al/TiB_2 IMC.

E. Microstructure Evolution during Spray Atomization and Deposition

On the basis of the previous discussion, it is evident that the cooling rate (1-10 K/s) present during the deposition stage is several orders of magnitude lower than that generally present during the atomization stage (10^3-10^5 K/s) [17, 20]. As a result, the deposited material will be exposed to a high temperature anneal for a finite period of time during deposition. Based on the high temperature annealing experiments described in the previous section, growth and coalescence phenomena will take place, leading to the formation of a spheroidal microstructure in the monolithic Ni_3Al and the formation of interfacial products in the Ni_3Al/TiB_2 IMC, during spray atomization and deposition. In addition, any phase transformation process which may occur during elevated temperature annealing, such as second phase formation, precipitation, etc., will occur as well in the material during the deposition stage.

On the basis of the aforementioned discussion, the different microstructural features that are present in regions A, B and C of the spray deposited material may be rationalized as follows. The microstructure present in the exterior bottom area (region A) of the deposit is dominated by the presence of powders that arrived on the substrate fully solidified. Recent studies on the measurement of droplet sizes during atomization using Doppler techniques [23] have shown that the peripheral region of the atomized spray is populated by droplets that are substantially smaller than those present in the center of the spray, and that the droplet mass flux decreases with

increasing distance from the spray axis. Consequently, small droplets in this region arrive on the substrate fully solidified, leading to the formation of thick prior-droplet-boundaries that remain unchanged during annealing. The elevated mass density associated with the center of the spray (region B) promotes a high degree of droplet deformation, leading to the formation of the thin prior-droplet-boundaries that were observed experimentally. Furthermore, the elevated temperature anneal experienced by this region allowed the growth and coalescence of dendrite fragments, leading to the formation of a spheroidal grain morphology by the mechanisms that were described previously. The material in region C was exposed to a similar thermal history as that present in region B, differing only in the rate of heat extraction, which was higher in this region as a result of the proximity of the water cooled substrate. As a result, the material present in this region exhibited a heterogeneous grain morphology, with associated prior-droplet-boundaries.

During synthesis of the Ni_3Al/TiB_2 IMC, the interaction between the reinforcement particulates and the matrix material also experienced two distinctive stages, i.e., atomization and deposition. During atomization, the experimental evidence suggests that heterogeneous nucleation occurred on the "cool substrate" of the reinforced particulate surface. Subsequently, the matrix material solidified rapidly around the TiB_2 particulates due to dynamic transfer of thermal energy to the atomization gas, and as a result, a relatively low temperature was maintained at the interface between TiB_2 and Ni_3Al [16, 28]. However, the sluggish cooling behavior experienced by the materials during the deposition stage provided sufficient thermal energy to kinetically activate interfacial reactions leading to the formation of a thermodynamically stable reaction product, such as the one described herein for the Ni_3Al/TiB_2 IMC. Presently, research efforts are aimed at investigating the mechanisms that govern interfacial behavior in a wide variety of metal/ceramic combinations.

F. Numerical Simulation of the Deposition Process

More recently, Liu et al. [31, 32] developed a numerical methodology to simulate the deformation and the solidification behavior of an individual semi-liquid droplet during impact onto a flat substrate. The numerical simulation was accomplished on the basis of the full Navier-Stokes equations and the Volume of Fluid (VOF) function, by using a 2-domain method for the thermal field and solidification problem and a two-phase flow continuum model for the flow problem associated with a growing solid layer. The calculated results demonstrated successfully that a droplet spreads uniformly in the radial direction during impingement onto a flat substrate and eventually forms a thin splat. Fig. 12(a) shows the calculated deformation sequence of an individual droplet, where the horizontal and vertical axes denote the length in meters. The final

diameter and height of the splat, which are critical to the geometric development and the microstructural changes in spray deposited materials, was suggested to depend on the impact velocity, viscosity, and surface tension of the droplets. The calculated results were in good agreement with the experimental values, see Fig. 12(b).

The results of the numerical calculation also suggests that with increasing initial impact velocity, the final diameter of the splat increases rapidly first, and the tendency slows down gradually. Droplets remain relatively undeformed when the viscosity and surface tension are considerably large. A fully liquid droplet impinging onto a solid substrate may lead to a good contact and adhesion between the splat and the substrate, whereas a fully liquid droplet striking onto another flattening, fully liquid splat produces ejection of the liquid. A fully liquid toroidal ring colliding with a flattening, fully liquid splat causes ejection of the liquid as well as the formation of voids. On the basis of this mechanism, some fundamental trends and effects of important processing parameters on micro-porosity may be reasonably explained and optimal processing conditions for dense deposited materials may be determined [31, 32].

G. Concluding Remarks

The application of spray atomization and deposition processing to synthesize elevated temperature materials such as intermetallic and intermetallic matrix composites, was motivated by the difficulties associated with the currently available casting and powder metallurgical processes. In principle, such an approach will inherently avoid the extreme thermal excursions with concomitant degradation in interfacial properties and extensive macrosegregation, normally associated with casting processes. Furthermore, this approach also eliminates the need to handle fine reactive particulates, as is necessary with powder metallurgical processes. The results reviewed in the present work demonstrate that the preliminary findings obtained with this synthesis approach are encouraging. It is also evident, however, that it will be necessary to develop an in-depth understanding of the fundamental physical phenomena involved, before such a process can measure up to its commercial potential. The latter will be a challenging task for the scientific community, in view of the complex fluid thermal and solidification phenomena involved.

H. References

1. N.S. Stoloff, "Physical and Mechanical Metallurgy of Ni_3Al and Its Alloys", *Int. Mater. Rev.*, 34(1989), pp. 153-189.
2. K. Aoki, "Ductilization of $L1_2$ Intermetallic Compound Ni_3Al by Microalloying with Boron", *Mater. Trans. JIM*, 31(1990), pp. 443-448.
3. R.W. Cahn, "Load-bearing Ordered Intermetallic Compounds - A Historical View", *MRS Bulletin*, (5)(1991), pp. 18-23.
4. C.T. Liu and V.K. Sikka, "Nickel Aluminides for Structural Uses", *J. Met.*, 38(5)(1986), pp. 19-21.
5 J.M. Yang, W.H. Kao and C.T. Liu, "Development of Nickel Aluminide Matrix Composites", *Mater. Sci. Eng.*, 107A(1989), pp. 81-91.
6. N.S. Stoloff and D.E. Alman, "Powder Processing of Intermetallic Alloys and Intermetallic Matrix Composites", *Mater. Sci. Eng.*, A144(1991), pp. 51-62.
7. J.H. Schneibel, E.P. George, C.G. McKamey, E.K. Ohriner, M.L. Santella and C.A. Carmichael, "Fabrication and Tensile Properties of Continuous-Fiber Reinforced Ni_3Al-Al_2O_3 Composites", *J. Mater. Res.*, 6(1991), pp. 1673-1679.
8. G.E. Fuchs, "The Chemical Compatibility and Tensile Behavior of an Ni_3Al-Based Composite", *J. Mater. Res.*, 5(1990), pp. 1649-1655.
9. A.R.E. Singer, "Recent Developments in the Spray Forming of Metals", *Met. Powder Rep.*, 41(1986), p. 117.
10. E.J. Lavernia, "The Evolution of Microstructure during Spray Atomization and Deposition", *Int. J. Rapid Solidification*, 5(1989), pp. 47-85
11. P. Mathur and A. Lawley, "Process Control, Modeling and Applications of Spray Casting", *JOM*, 41(10)(1989), pp. 23-28.
12. E.J. Lavernia, J.D. Ayers and T.S. Srivatsan, "Rapid Solidification Processing with Specific Application to Aluminum Alloys", *Int. Mater. Rev.*, 37(1992), pp. 1-44
13. X. Liang and E.J. Lavernia, "Solidification and Microstructure Evolution during Spray Atomization and Deposition of Ni_3Al", *Mater. Sci. Eng.*, A(1993) in press.
14. M. Gupta, F.A. Mohamed and E.J. Lavernia, "The Effect of Ceramic Reinforcements During Spray Atomization and Co-Deposition of MMCs", *Metall. Trans. A*, 23A(1992), pp. 831-850.
15. Y. Wu and E.J. Lavernia, "Spray-Atomized and Codeposited 6061 Al/SiC_p Composites", *JOM*, 43(8)(1991), pp. 32-35.

16. M. Gupta, F.A. Mohamed and E.J. Lavernia, "Heat Transfer Mechanisms and Their Effects on Microstructure during Spray Atomization and Codeposition of Metal Matrix Composites", *Mater. Sci. Eng.*, 144A(1991), pp. 99-110.
17. R. Mehrabian, "Rapid Solidification", *Int. Met. Rev., 24*(1982), pp. 186-208.
18. P. Mathur, D. Apelian and A. Lawley, "Analysis of the Spray Deposition Process", *Acta Metall.*, 37(1989), pp. 429-443.
19. E.M. Gutierrez, E.J. Lavernia, G.M. Trapaga, J. Szekely and N.J. Grant, "A Mathematical Model of the Spray Deposition Process", *Metall. Trans. A*, 20A(1989), pp. 71-85.
20. X. Liang, J.C. Earthman and E.J. Lavernia, "On the Mechanism of Grain formation during Spray Atomization and Deposition", *Acta Metall.*, 40(1992), pp. 3003-3016.
21. X. Liang, H.K. Kim, J.C. Earthman and E.J. Lavernia, "Microstructure and Elevated Temperature Behavior of a Spray Atomized and Co-deposited $Ni_3Al/SiC/TiB_2$ Intermetallic Matrix Composite", *Mater. Sci. Eng.*, 153A(1992), pp. 646-653.
22. X. Liang, and E.J. Lavernia, "Interfacial Behavior in a Ni_3Al/TiB_2 Intermetallic Matrix Composites", *Mater. Sci. Eng.*, 153A(1992), pp. 654-661.
23. B.P. Bewlay and B. Cantor, "Modeling of Spray Deposition - Measurements of Particle Size, Gas Velocity, Particle Velocity, and the Spray Temperature in Gas-Atomized Sprays", *Metall. Trans. B*, 21B(1990), pp. 899-912.
24. M.C. Flemings, "Behavior of Metal Alloys in the Semisolid State", *Metall. Trans. A*, 22A(1991), pp. 957-981.
25. X. Liang, J.C. Earthman, J. Wolfenstine and E.J. Lavernia, "A Comparison of Techniques for Determining the Volume Fraction of Particulates in Metal Matrix Composites", *Mater. Charact.*, 28(1992), pp. 173-178.
26. X. Liang, and E.J. Lavernia, "On the Dendrite-Equiaxed Grain Transition in Atomized Ni_3Al Powders", *Scr. Metall. et Mater.*, 25(1991), pp. 1199-1204.
27. R.W. Cahn, *Physical Metallurgy*, (North-Holland Publishing Co., 1970), p. 1129.
28. Y. Wu and E.J. Lavernia, "Interaction Mechanisms between Ceramic Particles and Atomized Metallic Droplets", *Metall. Trans. A*, 23A(1992), pp. 2923-2937.
29. S.T. Mileiko, in *Fabrication of Composites*, ed. A.Kelly and S.T. Mileiko, (North-Holland, New York, 1985), p. 221.
30. A.G. Metcalfe, *Interfaces in Metal Matrix Composites*, (Academic Press, New York, 1974), p. 66.
31. H. Liu, E. Muhlberger, A. Sickinger, E.J. Lavernia and R.H. Rangel, "Deformation and Interaction Behavior of Molten Droplets Impinging on a Flat Substrate in Plasma Spraying", in *Conf. Proc. of NTSC'93*, (ASM International, 1993), in press.
32. H. Liu et al., *Current Research in UCI*, 1993.

33. M. Kitaura, M. Yao, J. Senda and H. Fujimoto, in *Proc. of 13th Japanese Conference on Atomization of Liquids*, (1984).

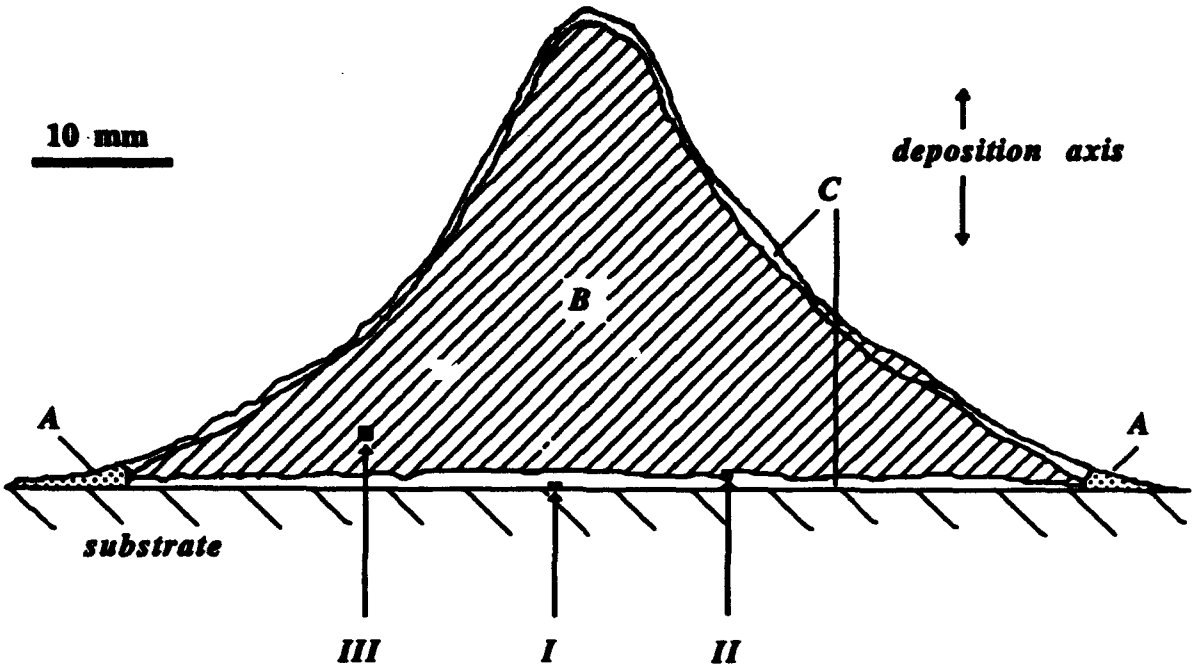

Fig. 1. Cross-section of as-deposited monolithic Ni_3Al billet and three regions A, B and C which reveal different microstructural morphology. I, II and III correspond to positions of three thermocouples [20].

(a)

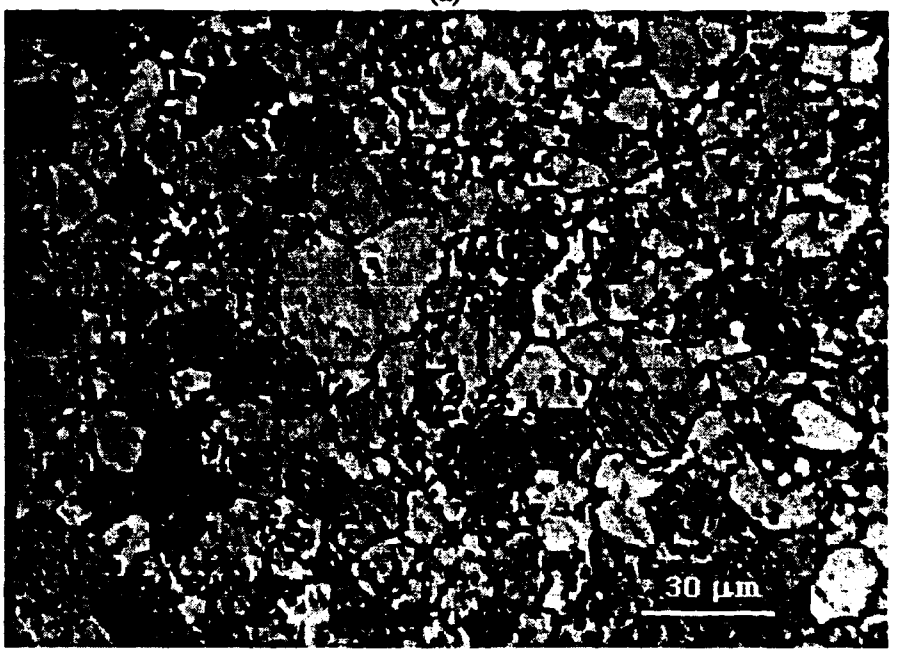

(b)

Fig. 2. (a) Layered microstructure showing deformed, fractured dendrites and thick prior-droplet-boundaries in region A. (b) Microstructure showing fine spheroidal grains in region B [20].

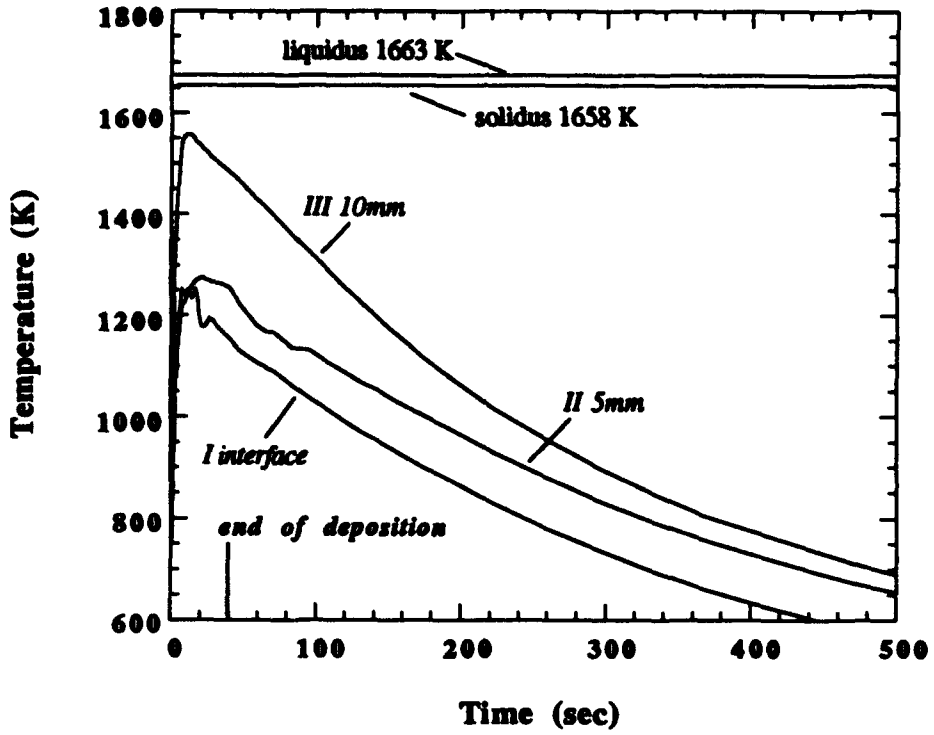

Fig. 3. Measured temperature profiles at three positions inside the deposit billet during spray atomization and deposition of Ni_3Al [20].

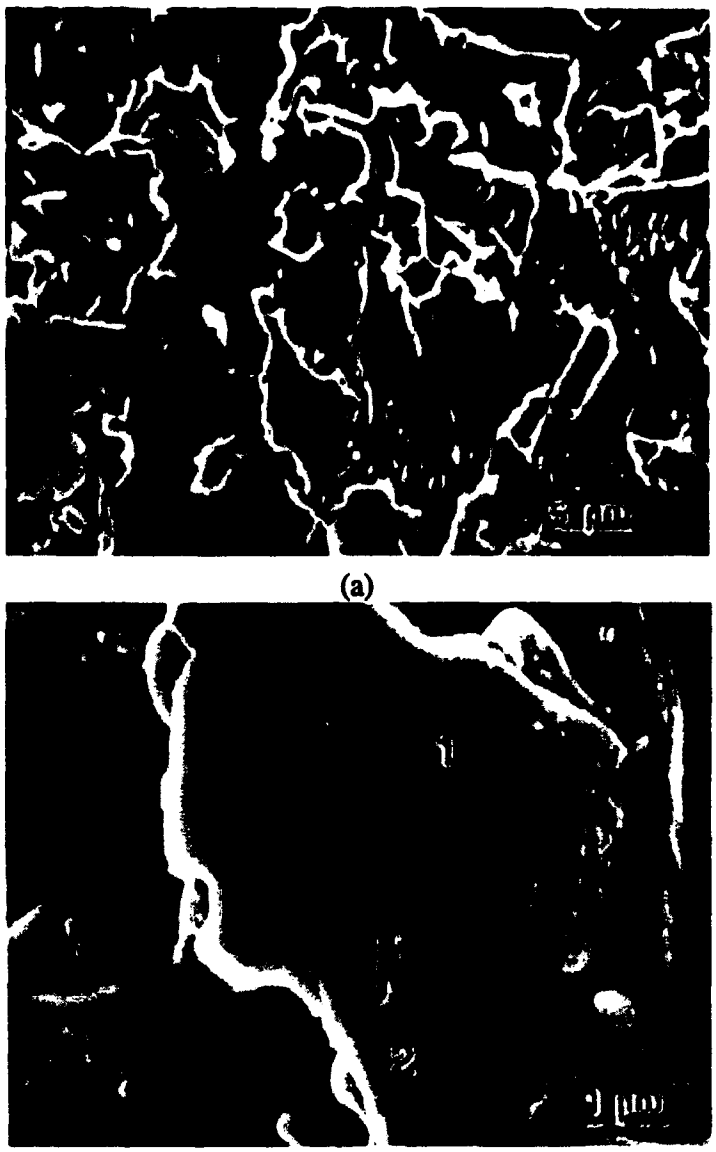

Fig. 4. (a) SEM micrograph showing the microstructure of the spray atomized and co-deposited Ni_3Al/TiB_2 IMC. (b) The interfacial reaction zone formed around the TiB_2 particulates [21, 22].

Fig. 5. The microstructure of Ni_3Al as-deposited materials (from region A) after annealing at 1403 K for 1 hour [20].

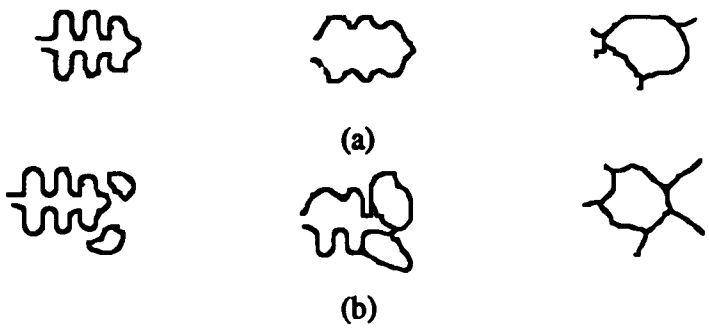

Fig. 6. Mechanisms leading to the formation of spheroidal grains during annealing: a) the homogenization of dendrites that did not deform extensively during deposition; and b) the growth and coalescence of the deformed or fractured dendrite arms [20].

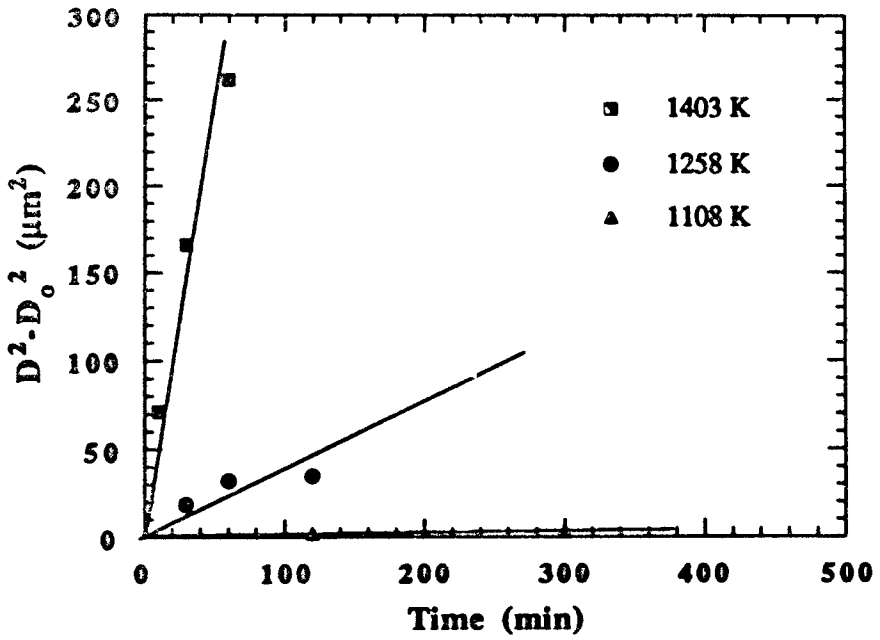

Fig. 7. The increase in dendrite fragment/spheroidal grain average diameter, D, relative to the original diameter (prior to annealing), D_o, as a function of annealing time [20].

(a)

(b)

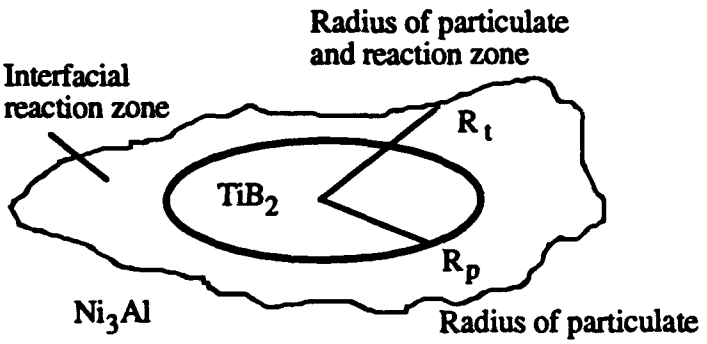

(c)

Fig. 8.(a) Microstructure in atomized Ni_3Al/TiB_2 powders (63 to 90 μm). (b) Interfacial reaction zone formed in atomized Ni_3Al/TiB_2 powders after annealing at 1403 K for 30 minutes. (c) Schematic diagram illustrating the determination of interfacial reaction zone thickness, i.e., R_t - R_p[22].

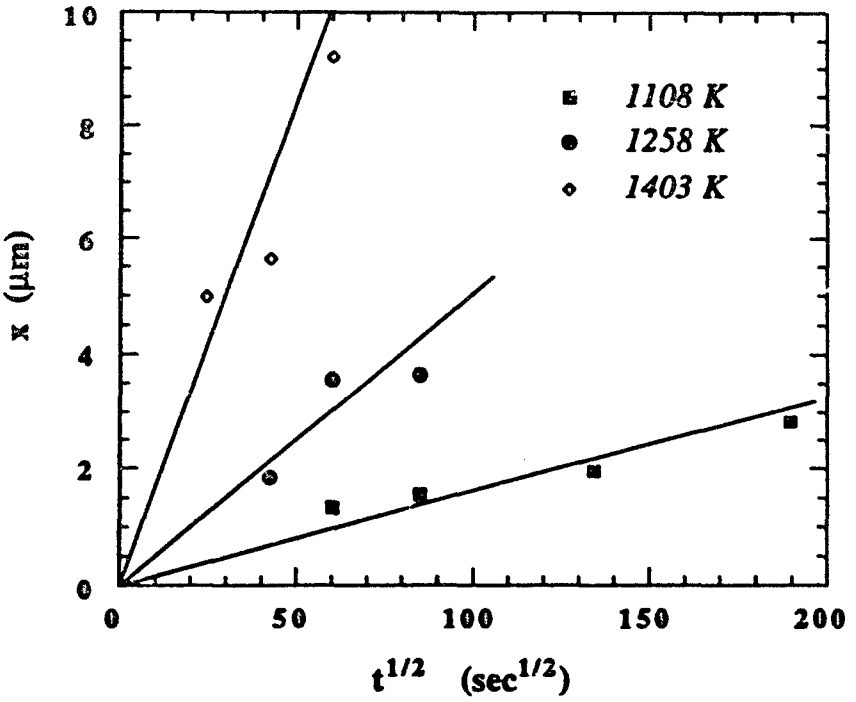

Fig. 9. Interfacial reaction zone thickness, x, as a function of annealing time, t, for three temperatures: 1108 K, 1258 K and 1403 K in Ni_3Al/TiB_2 IMC [22].

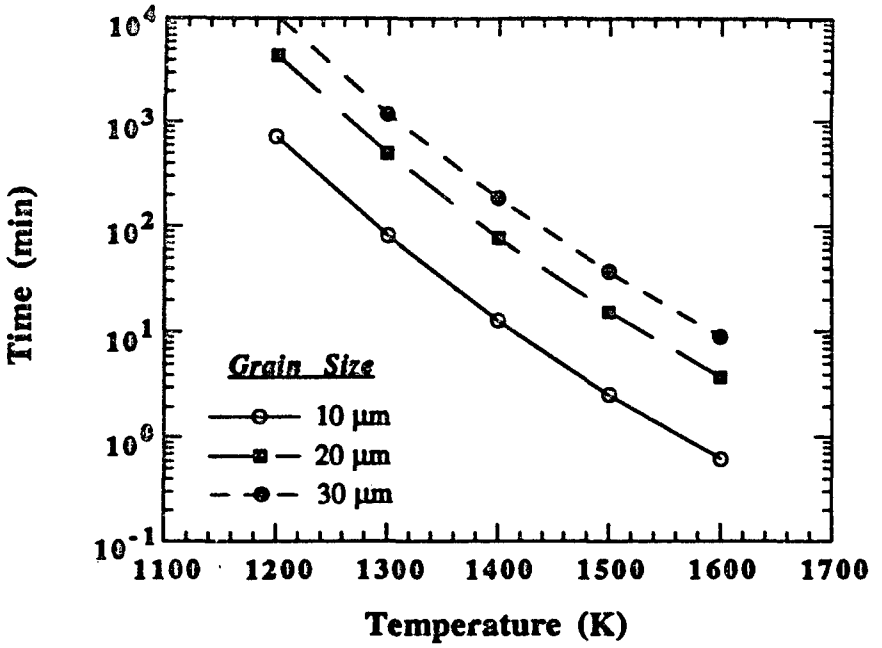

Fig. 10. Time and temperature required to achieve a particular grain size during annealing deposited Ni_3Al [20].

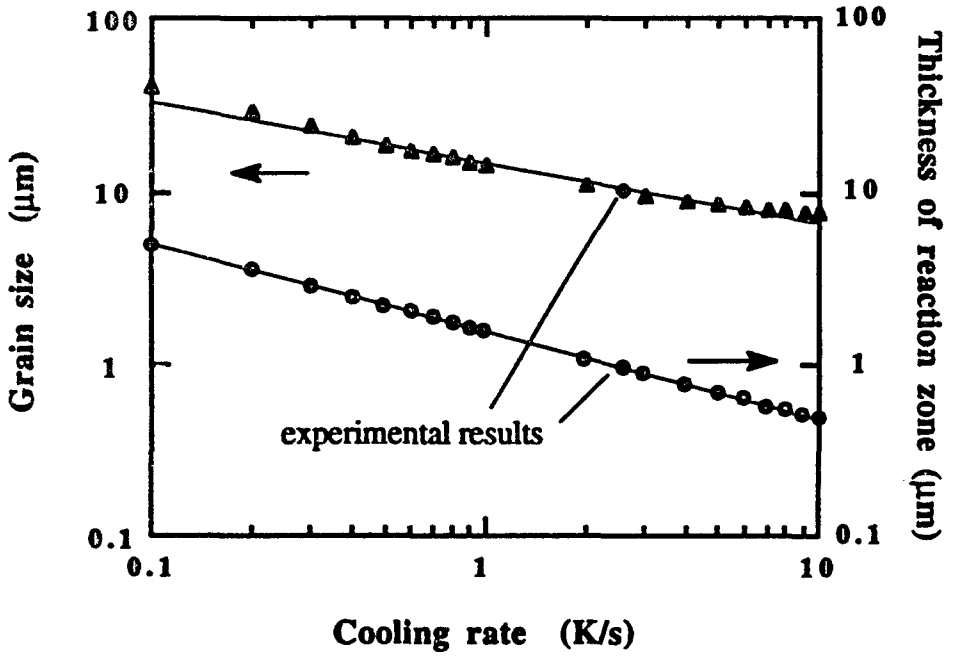

Fig. 11. The spheroidal grain size in as deposited Ni_3Al, and the interfacial reaction zone thickness between Ni_3Al and TiB_2 reinforcement in Ni_3Al/TiB_2 IMC versus the cooling rates [20].

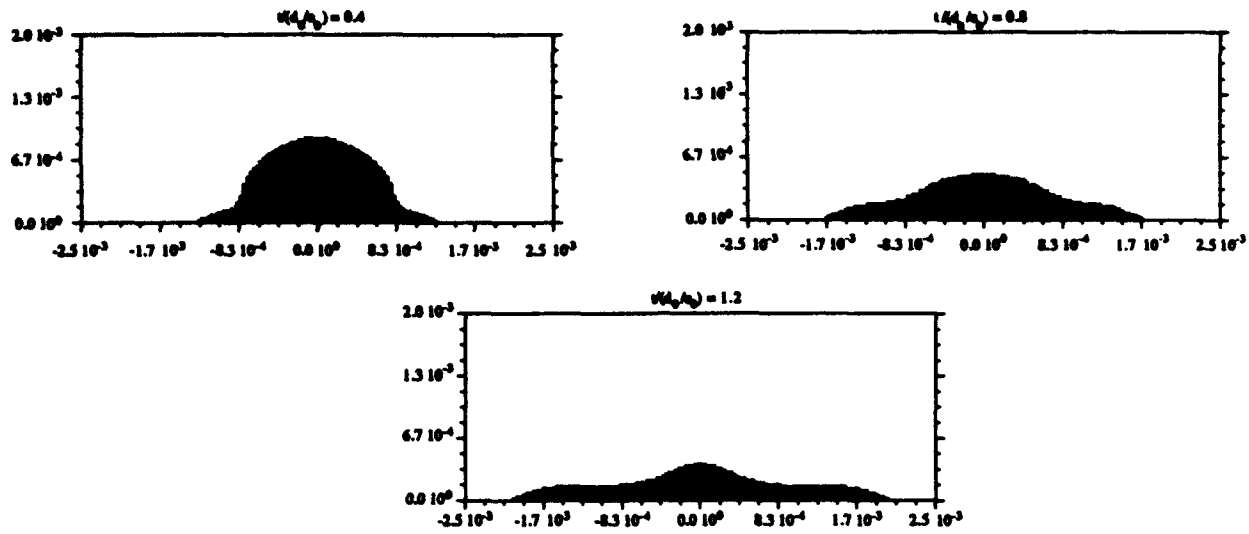

(a)

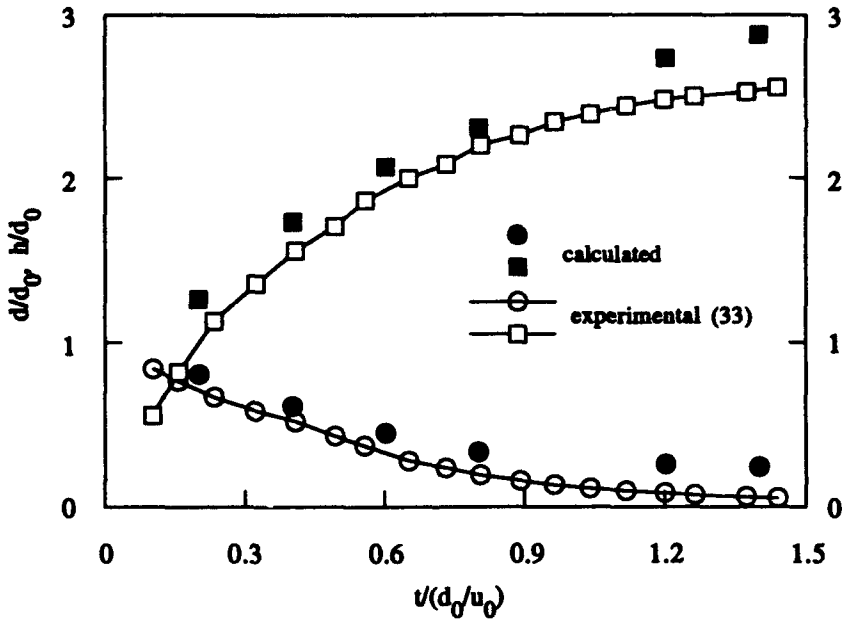

(b)

Fig. 12. (a) Calculated deformation sequence of a single droplet; (b) Comparison of the experimental and the calculated dimensionless height and diameter of the splat [31, 32].

III. High Temperature Rupture Mechanisms in a Particulate Reinforced Intermetallic Matrix Composite

A. Introduction

Intermetallic-matrix composites (IMCs) are potentially useful at elevated temperatures since they combine matrix properties of oxidation resistance and high temperature stability with reinforcement properties of high specific strength and modulus [1-8]. However, it is unlikely that these materials can be utilized successfully unless a better understanding of their high temperature properties is achieved. In particular, little is known about the nature of creep damage in these materials and whether or not the proposed reinforcement/matrix interfaces are susceptible to cavity formation and growth in the way that monolithic polycrystalline materials are susceptible to grain boundary cavitation.

It has been shown that creep rupture of monolithic Ni_3Al is facilitated by the nucleation, growth and coalescence of grain boundary cavities [9]. It follows that cavitation is also an important mechanism in the high temperature rupture of particulate reinforced Ni_3Al matrix composites. However, it is not immediately clear whether the most damaging cavitation occurs on the matrix grain boundaries or on the reinforcement/matrix interfaces. One of the factors adding to the uncertainty as to where in the microstructure the dominant damage would develop is the formation of interfacial reactions between matrix and reinforcement during both processing and service. It has been shown that the development of an interfacial reaction zone is often desirable for establishing good interfacial bonding. However, excessive growth of the interfacial reaction region can be detrimental to the mechanical properties of composites [10].

The objective of the present study was to develop a better understanding of the nature of creep rupture mechanisms in a Ni_3Al matrix composite produced by spray atomization and co-deposition. The selection of SiC particulates was prompted by the results of Chou and Nieh [11] which showed that strong solid state reactions developed between SiC and Ni_3Al, and multi-reaction-layers were always generated in the interdiffusion zone. Similarly, TiB_2 was reported to react with a Ni_3Al [12], there have been little information on the effect of the interfacial reaction zone on mechanical properties. Thus, it was also selected on the basis of the work by other investigators which suggests that this type of particulate provides attractive combinations of properties in IMCs [6]. By co-injecting both SiC and TiB_2 particulates in the same intermetallic matrix, it was possible to compare the role of both in the rupture process for the same matrix microstructure under identical conditions.

The high temperature properties of the monolithic Ni_3Al and $Ni_3Al/SiC/TiB_2$ IMC were compared on the basis of creep rupture times. Emphasis is placed on the roles of the reaction

products between the reinforcements and the matrix in affecting the mechanisms which facilitate high temperature fracture.

B. Procedures

B.1. Experimental Material

The nominal composition of the Ni_3Al used in the present study (ONRL designation IC-396) is 8.0 Al, 7.7 Cr, 0.85 Zr, 3.0 Mo, 0.005 B, bal Ni (in wt. pct.); the reinforcement SiC particulates (HCP α–phase) had an average size of 3 μm, whereas the TiB_2 particulates (C32 structure) had approximate average size of 15 μm prior to processing. During spray atomization and co-deposition, the Ni_3Al alloy was disintegrated into a dispersion of droplets using high energy N_2. Simultaneously, a mixture of TiB_2 and SiC particulates with the same volume fraction ratio was co-injected into the atomized spray at a previously determined spatial location. The primary experimental variables used in the processing procedure are given in [13]. For comparison, the same matrix material was spray deposited under the same conditions without the co-injection of the ceramic particulates.

Both the unreinforced Ni_3Al and Ni_3Al IMC were hot extruded to a ratio of 9:1 at 1473K to eliminate micrometer sized pores that normally develop during spray deposition. This treatment produced equiaxed grains with an average size of 10 μm in the composite indicating that dynamic recrystallization had taken place during hot extrusion. In contrast, a columnar grain structure resulted in the unreinforced Ni_3Al with an average grain length of 25 μm and a grain aspect ratio of 5. The volume fraction of ceramic particulates was quantitatively characterized using two techniques: (a) image analysis and (b) acid dissolution. The results from both techniques indicate a total ceramic particulate volume fraction of 12.7%. It is not possible to differentiate between the SiC and TiB_2 particulates in the photograph strictly on the basis of size and morphology. However, it is worth noting that the large particulates are most likely TiB_2, considering the initial size distributions of the SiC and TiB_2 particulates. It was also assumed that the composite was co-injected with approximately the same volume fraction of TiB_2 and SiC.

B.2. High Temperature Testing

Tensile creep specimens were ground to size with a gage diameter of 3.2 mm and a gage length of 15.9 mm. They were then tested under constant tensile stress conditions ranging from 180 to 350 MPa at 1033K in a vacuum environment of 10^{-3} Pa, using a custom-built automated high temperature testing system. Longitudinal sections of the specimens were examined using SEM techniques to determine the extent and location of creep damage within the microstructure of the experimental materials.

C. Results

C.1. Microstructural Observations

It was shown in Section I that a large number of carbides exist on the grain boundaries in the composite [13]. The observation that TiB_2 particulates are generally present at the grain boundaries of the matrix suggests that they hindered grain growth during hot extrusion. The chemical reaction products at the Ni_3Al/TiB_2 interface are described in Section I. Finally, it is noted that microvoids were observed within the interface region which were 0.4 - 0.9 μm long and 0.1 - 0.4 μm wide.

Although X-ray diffraction studies conducted on the composite revealed the presence of SiC [13], these particulates were not evident from scanning electron microscope (SEM) observations combined with and EDS analysis. It appears that the SiC particulates were substantially reduced in size or eliminated during both the spray deposition and extrusion processing steps. In related studies, Chou and Nieh [11] noted that SiC reacts extensively with pure Ni_3Al during annealing at 1273K, leading to the formation of multiple reaction layers in the interdiffusion zone at the interface. It appears that the temperatures during deposition (1100-1600K) provide sufficient thermal energy for the alloying elements Cr, Mo, Zr to segregate to the Ni_3Al/SiC interface. These alloying elements are then able to replace the Si in the SiC lattice leading to the formation of other carbides. Concurrent diffusion of Si into the Ni_3Al matrix may also lead to the formation of compounds with Ni and Al, as reported by Chou and Nieh [11]. The high surface to volume ratio associated with the fine (3 μm) SiC particulates was also a factor that contributed towards their high reactivity.

C.2. Creep Behavior

Typical creep curves for specimens tested under 300 MPa are illustrated in Figure 1. Data for spray deposited and extruded monolithic Ni_3Al specimens are included for comparison. Steady state strain rate is plotted against applied stress in Figure 2 for bothcomposite and monolithic Ni_3Al specimens. Least square fit analyses of the data in this figure give Norton law constants of

$$\dot{\varepsilon} = 3.4 \times 10^{-16} \sigma^{3.44} \quad \text{for monolithic } Ni_3Al$$

$$= 1.2 \times 10^{-15} \sigma^{3.50} \quad \text{for } Ni_3Al/SiC/TiB_2$$

where strain rate, $\dot{\varepsilon}$, and applied stress, σ, are in units of s^{-1} and MPa, respectively. The experimental data reveal that the stress exponent for power law creep for both materials is approximately 3.5, suggesting that the creep deformation for both materials is predominantly

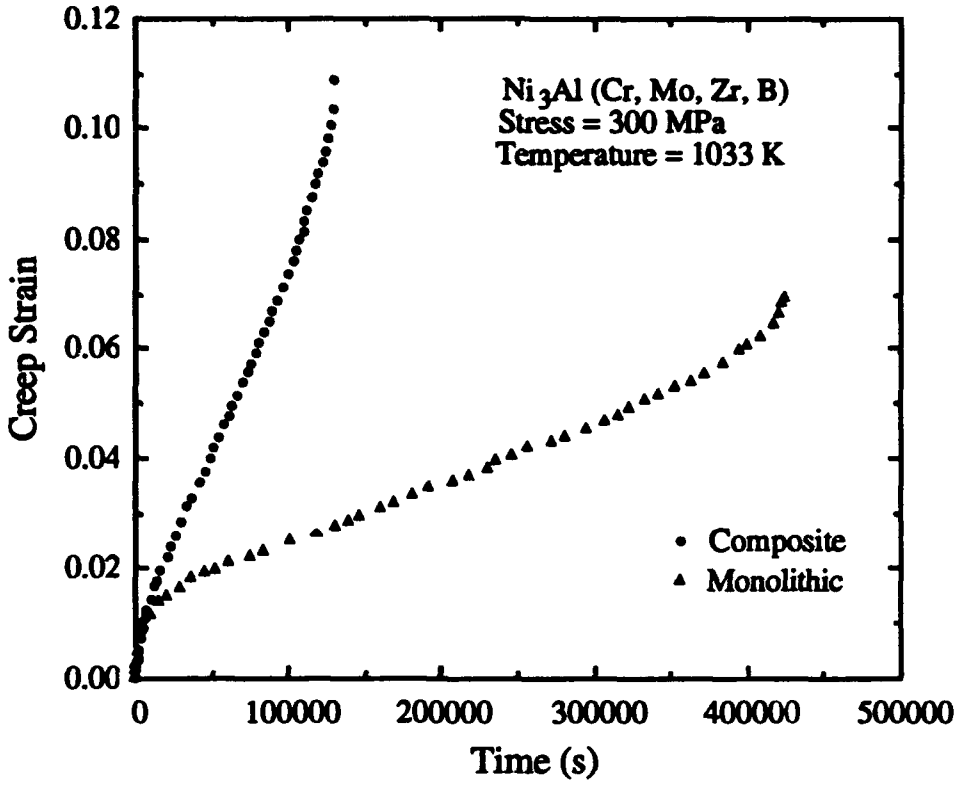

Figure 1. Typical creep curves for the monolithic and composite materials.

controlled by dislocation glide processes. It is not immediately clear why the creep rate of the composite is about six times faster than that for the unreinforced Ni_3Al for a given stress. Composite hardening is known to be due to a difference in plastic strain of the components compensated by elastic strains which give rise to back stresses. It is often assumed that there is no difficulty in transferring load between matrix and reinforcement in order to prevent the development of local incompatibility stresses. The shear-lag theory [14] can be used to predict composite strength, even though the reinforcing phase possesses a small aspect ratio as in the case of a particulate reinforced Al matrix composite [15]. However, weak interfaces can have a substantial effect on this load transfer and, as a result, on the creep behavior of composites. In the limit of zero interface strength, where no load can be transferred to the reinforcement, a composite is weaker than the matrix alone [16]. As mentioned before, the processing of the composite apparently results in the decomposition of the SiC particulates and the formation of other carbide phases, such as Cr_3C_2-type carbides, and the formation of the Ni-rich interfacial phase at the Ni_3Al/TiB_2 interface. This could give rise to a weakening of the interfaces present in the composite.

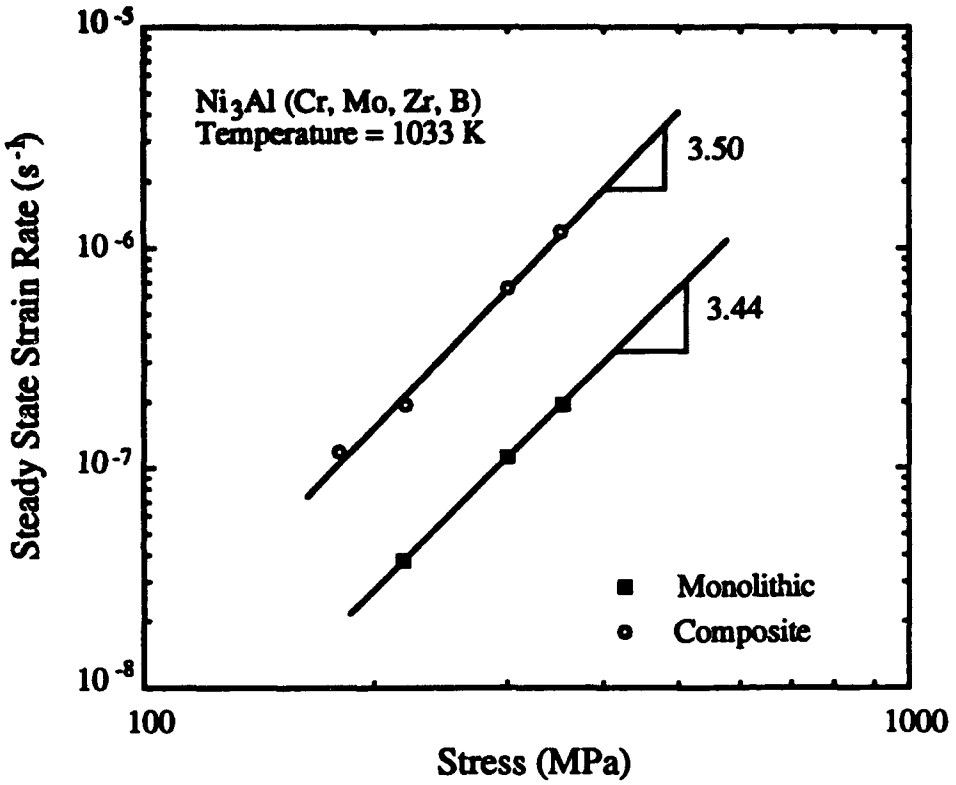

Figure 2. Strain rate versus applied stress for the monolithic and composite materials.

Flinn [17] has proposed that the steady-state creep of $Ni_3(Al, Fe)$ polycrystals for the temperature range used in the present investigation is controlled the viscous drag on dislocation pairs associated with the antiphase boundary (APB) connecting the members of the pair. Since therate-controlling process is the diffusion of atoms to and from the APBs, impurity elements affecting lattice diffusion could play a role in the creep behavior of Ni_3Al. In this case, impurity elements in a composite may increase lattice diffusion and therefore increase the creep rate. It is likely that the present composite contains significant amounts of Si, resulting from the decomposition of SiC, which could then increase lattice diffusion. It is also possible that the precipitation of another soft phase containing Si or C might attribute to the weaker creep strength of the composite compared to that for the monolithic material.

The finer and more equiaxed grain size present in the composite relative to that of the monolithic material may also account for the faster creep rate of the composite, if grain boundary sliding makes a significant contribution to the overall straining of the specimens. The shear stresses on grain boundaries would be generally lower in the monolithic material due to the more columnar grain morphology. Thus grain boundary sliding would likely have a negligible role in

contributing to the creep rate and redistributing stresses from inclined sliding inclined boundaries to cavitating boundaries that are transverse to the applied tensile stress.

C.3. High Temperature Rupture

Figure 3 shows a double logarithmic plot of creep rupture lifetime for both monolithic and particulate reinforced Ni_3Al as a function of applied stress. The monolithic material exhibits a longer lifetime than the composite for the same applied stress in this plot. This finding suggests that the mechanism which causes rupture is assisted by the presence of the reinforcing particulates. We note for the monolithic material that the rate equations for the rupture time and the steady state strain rate have a similar dependence on stress. In this case it is reasonable that the creep and fracture processes are closely linked. That is, at the same temperature:

$$t_r = A'\sigma^{-n'} \tag{1}$$

and

$$\dot{\varepsilon} = A\,\sigma^{n} \tag{2}$$

where t_r is the rupture time, A, A', n and n' are constants. For the monolithic material $n = 3.44$ and $n' = 3.2$. The composite, on the other hand, appears to undergo a different creep fracture process than is observed for the monolithic spray deposited material since the data indicate that $n \neq n'$ for this material. This suggests that processes other than dislocation creep also influence the rupture process for the composite. Observations of creep damage are discussed in the following section that support this finding.

C.4. Microstructural Observations

Cavity nucleation is generally favored at locations where diffusion is rapid and atomic bonding is relatively weak. Accordingly, reinforcement/matrix interfaces as well as the matrix grain boundaries represent possible preferred cavity nucleation sites in the present IMC. Thus, in order to develop a better understanding of the rupture mechanisms in this material it is first necessary to determine at which of these locations cavities nucleate preferentially. Longitudinal sections of ruptured specimens have been examined using SEM to determine the extent and location of creep damage within the microstructure of the composite. These observations were made on tested material from the grip sections of specimens which experienced a relatively low stress (approximately less than 25% stress in gage section region due to the increase in the cross-section area) during testing. This was done to avoid difficulties in identifying the preferred cavity nucleation sites in the extensively damaged gage sections.

A typical SEM micrograph of tested grip section material from a composite specimen tested under 300 MPa is shown in Figure 4. As indicated in this micrograph, larger cavities are

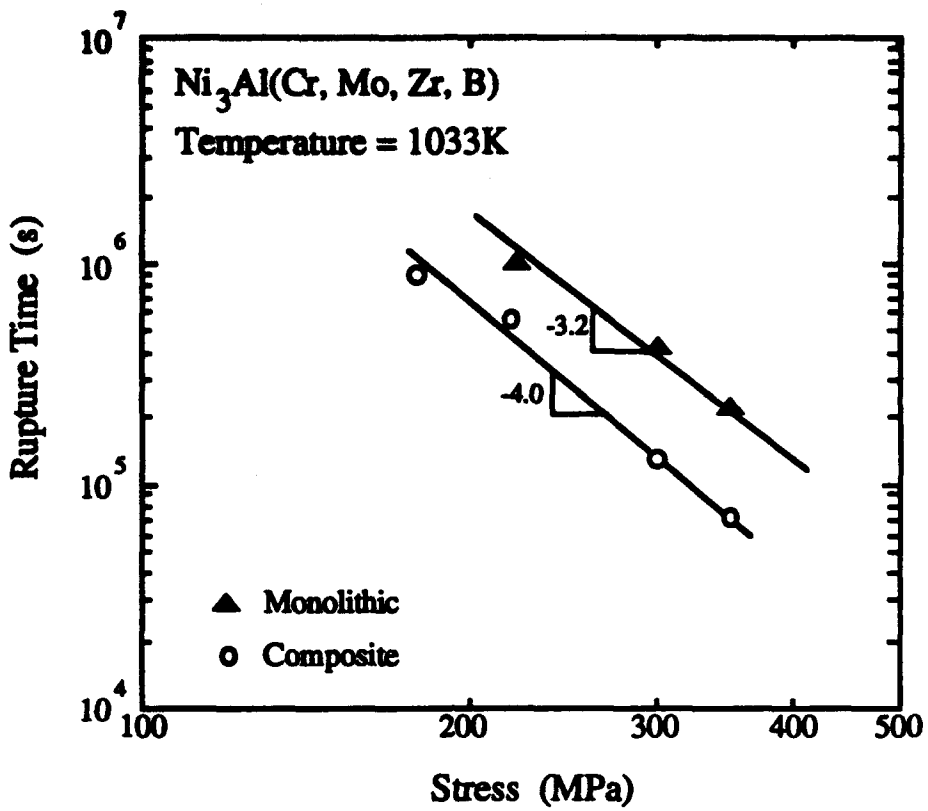

Figure 3. Rupture time versus applied stress for the monolithic and composite materials at 1033K.

observed at the Ni_3Al grain boundaries as opposed to TiB_2/Ni_3Al interfaces of comparable size and orientation. As mentioned previously, a large number of carbides exist on the grain boundaries in the composite [13]. Apparently, the grain boundary cavities nucleated at fine carbides which resulted from the decomposition of SiC particulates. It is possible that the nucleation of grain boundary cavities at the carbides occurs easily due to a relatively weak interfacial cohesive strength. On the other hand, the rare presence of large cavities at the Ni_3Al/TiB_2 reaction zones indicates that cavity formation is slow at these interfaces. This finding is consistent with the microstructural observations of coherent interfacial bonding along the Ni_3Al/TiB_2 interface reported in an earlier work [13]. A representative micrograph of gage section material is shown in Figure 5 for a specimen tested to rupture under 180 MPa. Again in this figure we note that more cavities appear to lie on the matrix grain boundaries than on the Ni_3Al/TiB_2 interfaces. It is also apparent that the grain boundary cavities are larger than those on the interfaces. This observation is confirmed in a plot of relative cavity frequency versus cavity size for both grain boundaries and matrix/TiB_2 interfaces illustrated in Figure 6. Each distribution in this figure was determined from approximately 300 cavities from a number of fields

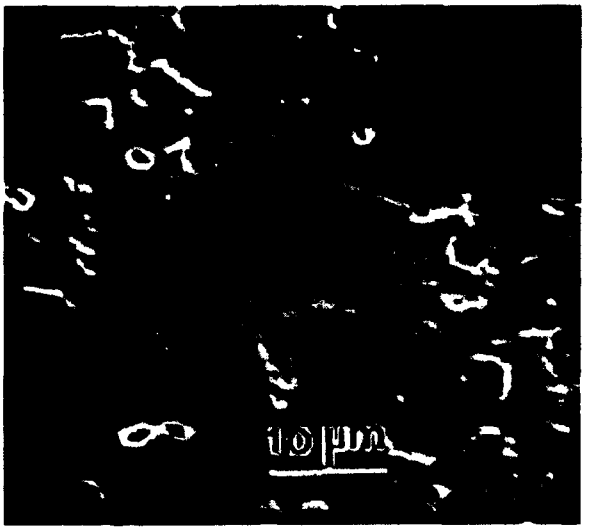

Figure 4. SEM micrograph of a region in the grip section of a composite specimen tested under 300 MPa. The tensile stress axis is in the vertical direction for this micrograph.

on the gage section using SEM techniques in conjunction with computer-based image analysis. A comparison of the mean cavity size of 1.3 μm for the grain boundaries and 0.7 μm for the Ni_3Al/TiB_2 interfaces indicates that the overall size of the cavities on the grain boundaries is larger than that for the cavities on the interfaces. However, it can be seen in Figure 6 that the overall frequency of cavities at matrix/TiB_2 interfaces was somewhat higher than that for the matrix grain boundaries. This indicates that a significant number of cavity nucleate on the matrix/reinforcement interfaces during the life of the specimens. Nonetheless, it appears the cavity growth at the matrix grain boundaries is faster making it the dominant damage mode in determining the life of the specimens.

The overall results indicate that it is the Ni_3Al grain boundaries, and not the Ni_3Al/TiB_2 interfaces, that are most susceptible to creep cavitation damage in the present composite. One possible explanation for this finding is that the carbide precipitates resulting from the dissolution of SiC enhance the cavity nucleation process at the grain boundaries. Cavity nucleation at iron carbides has been well documented for several steel alloys [18, 19]. Grain boundary carbides in the present IMC could also serve as preferred nucleation sites. Although large interfacial reaction zones form at the Ni_3Al/TiB_2 interfaces, they do not appear to cavitate as readily as the matrix grain boundaries. Thus, it is expected that a Ni_3Al matrix composite containing only TiB_2 could have a resistance to high temperature fracture that is comparable to monolithic Ni_3Al with the advantages of higher a strength-to-weight ratio and stiffness provided by the reinforcement.

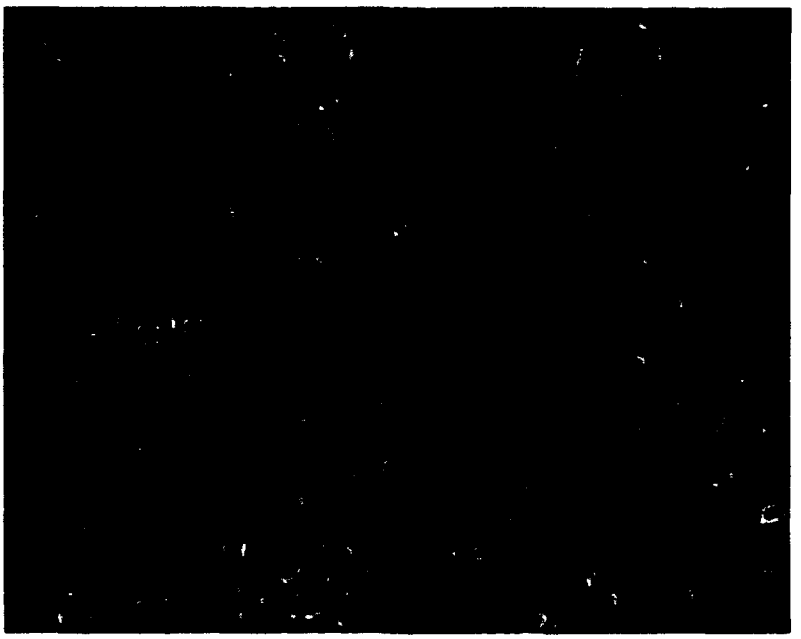

Figure 5. SEM micrograph of a region in the gage section of the composite specimen tested under 180 MPa. The tensile axis is in the vertical direction for this micrograph.

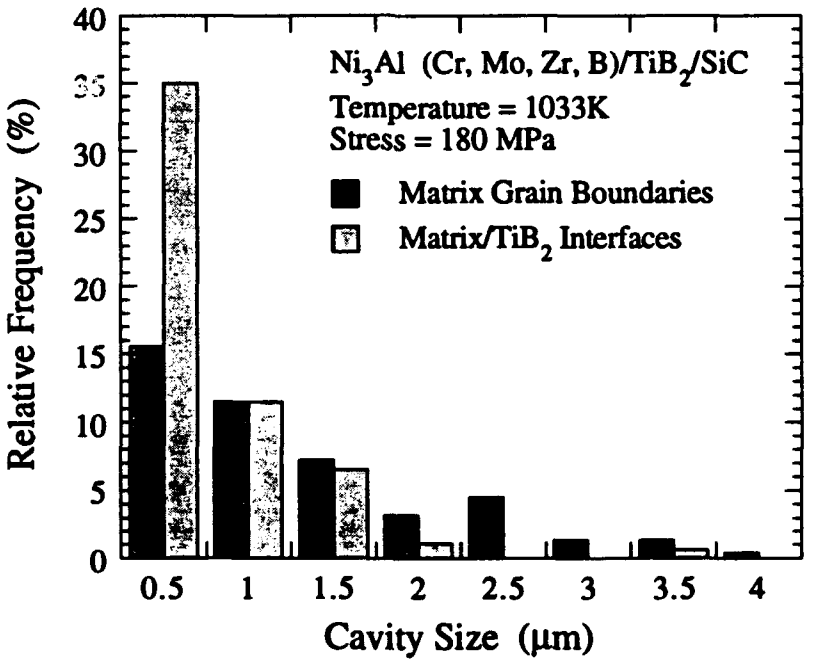

Figure 6. Relative frequency versus cavity size for both matrix grain boundaries and Ni_3Al/TiB_2 interfaces in the composite specimen tested under 180 MPa.

D. Conclusions

i) The stress exponent for power law creep for both unreinforced and particulate reinforced Ni_3Al produced by spray deposition is about 3.5, suggesting that the creep mechanisms for both materials are primarily controlled by dislocation glide processes. However, the composite specimens crept faster than the unreinforced Ni_3Al. It appears that differences in the grain morphology are responsible for this difference in creep behavior. Also, soft phases resulting from the decomposition of SiC in the composite could contribute to this disparity.

ii) Monolithic Ni_3Al exhibits longer creep lifetimes than that for the present Ni_3Al matrix composite. The stress exponent magnitudes for the monolithic Ni_3Al he composite exhibits different stress exponent magnitudes for minimum strain rate and rupture time indicates that mechanisms other than dislocation creep have a significant effect on the rupture time. It also suggests that the dissolution of SiC has substantially altered the creep rupture behavior of the matrix.

iii) Microstructural observations indicate that the cavity growth rates on Ni_3Al grain boundaries exceeded that for cavities on the Ni_3Al/TiB_2 interfaces. Since grain boundary cavities appear to nucleate at carbides resulting from the dissolution of SiC, it is apparent that longer lifetimes could be achieved if TiB_2 is co-injected as the sole reinforcement phase for the present Ni_3Al alloy.

E. References

1. N.S. Stoloff, *Inter. Mat. Rev.*, 34, 153 (1989).
2. K. Aoki and O. Izumi, *J. Jpn. Inst. Met.*, 43, 1190 (1979).
3. V.K. Sikka, *in Casting of Near Net Shape Products*, ed. Y. Sahai, J.E. Battles, R.S. Carbonara and C.E. Mobley, AIME, Warrendale, PA, 315 (1988).
4. C.T. Liu and V.K. Sikka, *J. Met.*, 5, 19 (1986).
5. K. Aoki, Mater. Trans. *JIM*, 31, 443 (1990).
6 J.M. Yang, W.H. Kao and C.T. Liu, *Mater. Sci. Eng.*, 107A, 81 (1989).
7. S. Nourbakhsh, F.L. Liang and H. Margolin, *Adv. Mat. & Manuf. Pro.*, 34, 57 (1988).
8. G.L. Povirk, J.A. Horton, C.G. McKamey and T.N. Tiegs, *J. Met. Sci.*, 23, 3945 (1988).
9. J.H. Schneibel and L. Martinez, *Acta Metall.*, 37, 2237 (1989).
10. T.W. Chou, A. Kelly and A. Okura, *Composite*, 16, 187 (1985).
11. T.C. Chou and T.G. Nieh, *J. Mater. Res.*, 5, 1985 (1990).
12. P. Angelilni, P.F. Becher, J. Bentley, C.B. Finch and P.S. Sklad, in J.H. Crawford, Y. Chen and W.A. Sibley (eds.), *Dect Properties and Processing of High-Technology Nonmetallic Materials*, Materillals Research Society, Pittsburgh, PA, 299 (1984)
13 X. Liang, H.K. Kim, J.C. Earthman and E.J. Lavernia, *J. Mater. Sci. & Eng.*, in press.
14. A. Kelly and K.N. Street, *Proc. R. Soc. Lond.*, 328A, 267 (1972).
15. K.T. Park, PH.D. Disertation, University of California, Irvine, (1992).
16. S. Goto and M. McLean, *Acta Metall.*, 39, 165 (1991).
17. P.A. Flinn, *Trans. Met. Soc. AIME*, 218, 145 (1960).
18. E.P. George, P.L. Li and D.P. Pope, *Proc. of the Conference on Creep and Fracture of Engineering Materials and Structures*, Swansea, Inst. of Metals, London (1987).
19. G. Eggeler, J.C. Earthman, N. Nilsvang and B. Ilschner, *Acta Metallurgica*, 37, 49 (1989).

ORAL PRESENTATIONS RESULTING FROM AFOSR GRANT NO. 90-036 DURING THE FINAL REPORTING PERIOD

(March 1, 1993 to February 28, 1994)

1. X. Liang and E.J. Lavernia, "On The Microstructure of $Ni_3Al/SiC/TiB_2$ Intermetallic Matrix Composites Processed by Spray Atomization and Co-Deposition," *Symposium on Structure Property Relationships for Metal/Metal Interfaces*, Materials Research Society Meeting, 1991.*

2. X. Liang, J.C. Earthman and E.J. Lavernia, "Interfacial Behavior in Ni_3Al/TiB_2 Intermetallic Matrix Composites," *Advanced Metal Matrix Composites for Elevated Temperatures*, 1991.*

3. X. Liang, J.C. Earthman and E.J. Lavernia, "Microstructure and High Temperature Behavior of a Spray Atomized and Co-Deposited Ni_3Al/TiB_2 Intermetallic Matrix Composite," in *Advanced Metal Matrix Composites for Elevated Tempearures*, M. Gungor, E.J. Lavernia, and S. G. Fishman, eds., TMS, Warrendale, PA, pp. 121-127, 1991.*

5. X. Liang, A. Campo and E.J. Lavernia, "Solidification and Heat Transfer Aspects of Non-Equilibrium Processing of Advanced Structural Materials," in conference proceedings, *Encontro Nacional de Ciencias Termicas,* Rio de Janeiro, Brazil, December 1-7, in press, 1992.*

6. H. Kim, X. Liang, J.C. Earthman, and E.J. Lavernia, "High Temperature Rupture Mechanisms in a Particulate Reinforced Intermetallic Matrix Composite," in conference proceedings, *Symposium on Processing, Fabrication and Performance of Composite Materials II* , T.S. Srivatsan and E.J. Lavernia, eds., American Society of Mechanical Engineers, Winter Annual Meeting, Anaheim, CA, (1992).*

7. K. J. C. Chou and J. C. Earthman, "Analysis of a Dendritic Ni_3Al Alloy by X-Ray Diffraction," *International Conference on High-Temperature Intermetallics*, San Diego, May 16-19, 1994.

* Although these presentations were given before the final reporting period, they were not reported previously and are therefore included in the present list.

PUBLICATIONS RESULTING FROM AFOSR GRANT NO. 90-0366 DURING THE FINAL REPORTING PERIOD

(March 1, 1993 to February 28, 1994)

1. X. Liang and E.J. Lavernia, "Interfacial Behavior in Ni_3Al/TiB_2 Intermetallic Matrix Composite," *Materials Science and Engineering,* A153, 654-661 (1992).*

2. X. Liang, J.C. Earthman and E.J. Lavernia, "On The Mechanism of Equiaxed Grain Formation During Spray Atomization and Deposition," *Acta Metallurgica et Materialia,* 40, 3003-3016 (1992).*

3. X. Liang and E.J. Lavernia, "Residual Stress Distribution in Spray Atomized and Deposited Ni_3Al," *Scripta Metallurgica et Materialia,* 29, 353-358 (1993).

4. H. K. Kim and J. C. Earthman, "High Temperature Deformation and Fracture Mechanisms in a Dendritic Ni_3Al Alloy," *Acta Metallurgica et Materialia,* 42, 679-688 (1994).

5. J. Wolfenstine, H. K. Kim and J. C. Earthman, "Creep Characteristics of Single Crystalline $Ni_3Al(Ta,B)$" accepted for publication in *Metallurgical Transactions.*

* Although these papers were published before the final reporting period, they were not reported previously and are therefore included in the present list.

PERSONNEL DURING THE FINAL REPORTING PERIOD

Principal Investigator:

J. C. Earthman, Assistant Professor

Co-Principal Investigator:

E. J. Lavernia, Associate Professor

Graduate Research Assistants:

K. J. C. Chou, Ph. D. candidate

D. E. Lawrynowicz

X. Liang, Ph. D. candidate